Non-Invasive Methods To Detect Underground Leaks

by

Siddhant Srivastava

A Thesis Presented in Partial Fulfillment
of the Requirements for the Degree
Master of Science

Approved July 2019 by the
Graduate Supervisory Committee:

TaeWoo Lee, Chair
Beomjin Kwon
Jeonglae Kim

ARIZONA STATE UNIVERSITY

August 2019

ABSTRACT

Water is one of, if not the most valuable natural resource but extremely challenging to manage. According to old research in the field, many Water Distribution Systems (WDSs) around the world lose above 40 percent of clean water pumped into the distribution system because of unfortune leaks before the water gets anywhere from the fresh water resources. By reducing the amount of water leaked, distribution system managers can reduce the amount of money, resources, and energy wasted on finding and repairing the leaks, and then producing and pumping water, increase system reliability and more easily satisfy present and future needs of all consumers. But having access to this information pre-amatively and sufficiently can be complex and time taking. For large companies like SRP who are moving tonnes of water from various water bodies around phoenix area, it is even more crucial to efficiently locate and characterize the leaks. And phoenix being a busy city, it is not easy to go start digging everywhere, whenever a loss in pressure is reported at the destination.

Keeping this in mind, non-invasive methods to geo-physically work on it needs attention. There is a lot of potential in this field of work to even help with environmental crisis as this helps in places where water theft is big and is conducted through leaks in the distribution system. Methods like Acoustic sensing and ground penetrating radars have shown good results, and the work done in this thesis helps us realise the limitations and extents to which they can be used in the phoenix are.

The concrete pipes used by SRP are would not be able to generate enough acoustic signals to be affectively picked up by a hydrophone at the opening, so the GPR would be helpful in finding the initial location of the leak, as the water around the leak

would make the sand wet and hence show a clear difference on the GPR. After that the frequency spectrum can be checked around that point which would show difference from another where we know a leak is not present.

ACKNOWLEDGMENTS

This thesis would not have been possible without the assistance and guidance of two individuals who in one way or another contributed their valuable assistance in the preparation and completion of this study.

First and foremost my utmost gratitude to my advisor and committee chair Dr. T.W.Lee, associate professor in the mechanical and aerospace engineering department whose knowledge and encouragement I will always remember. Dr. Lee always strove to make sure that I maintained a steady work pace so as to meet the sponsoring company's deadlines, Salt River Project, and ensure that they were given information that would greatly aid them in their research on this topic. Dr. Lee's vast knowledge in thermodynamics and fluid mechanics greatly helped in determining the most useful method for presenting the results of this study.

Kevin Hargrave, another mechanical and aerospace engineering graduate student, whose help in running and analyzing several of the simulation cases, especially the temperature validation cases, helped to alleviate some of the burden of CFD research. Kevin was also a major asset in preparing the industrial report for the sponsoring company, SRP, when it was time to deliver the results.

I would also like to thank SRP for their continued financial support of this research and their patience. I would also like to thank Mr Elsaad Hassan for his support and help in letting us use the SRP pipes and locations to conduct tests on the field.

TABLE OF CONTENTS

Page

LIST OF TABLES v

LIST OF FIGURES vi

LIST OF SYMBOLS / NOMENCLATURE ix

CHAPTER

1 INTRODUCTION 1

2 METHODOLOGY 4

Acoustic Sensing 4

Ground Penetrating Radar 20

3 RESULTS 31

Acoustic Sensing 31

Ground Penetrating Radar 48

4 CONCLUSION 69

5 REFERENCES 71

APPENDIX

A: MATLAB CODE FOR ANALYZING THE AUDIO SIGNALS 73

LIST OF TABLES

Table Page

1. Depth reached depending on soil of Arizona - dielectric 23.....27

2. General properties of materials 28

3. Sound recording parameters and quality.....31

LIST OF FIGURES

Figure Page

1. Test section setup where 2 Inch diameter pipe into the 4 inch pipe.....5

2. 1/4 , 1/16 and 1/8 inch leak.....6

3. Another look at the setup.....6

4. Hydrophone, DolphinEar *PRO* Series.....7

5. Audio USB interface, behringer u-phoria umc22.....7

6. Division of 1 signal of 16 points into 16 signals of 1 point.....12

7. Binary representation of the signal.....13

8. Functioning of the conversion from time domain to frequency domain.....15

9. Mixing of the odd and even spectrum.....16

10. Multiplication of the sinusoid.....17

11. Conversion from time domain to frequency domain.....19

12. Desert gold ground penetrating radar.....20

13. Working principle of the ground penetrating radar.....23

14. Generation of traces through the GPR.....25

15. Schematic of the test section with hydrophone at the first location.....33

16. FFT and power spectrum for the setup with Mic at Location 1 and No leak opened 34

17. FFT and power spectrum for the setup with Mic at Location 1 and 1/4" inch leak opened 34

18. FFT and power spectrum for the setup with Mic at Location 1 and 1/16” leak opened 35

19. FFT and power spectrum for the setup with Mic at Location 1 and 1/8” leak opened 35

Figure Page

20. FFT and power spectrum for the setup with Mic at Location 1 and All leaks opened 36

21. Schematic of the test section with hydrophone at the second location.....37

22. FFT and power spectrum for the setup with Mic at Location 2 and No leak opened 37

23. FFT and power spectrum for the setup with Mic at Location 2 and 1/4" leak opened 38

24. FFT and power spectrum for the setup with Mic at Location 2 and 1/16” leak opened 38

25. FFT and power spectrum for the setup with Mic at Location 2 and 1/8” leak opened 39

26. FFT and power spectrum for the setup with Mic at Location 2 and All leaks opened 39

27. Schematic of the test section with hydrophone at the third location.....43

28. FFT and power spectrum for the setup with Mic at Location 3 and no leak opened 43

29. FFT and power spectrum for the setup with Mic at Location 3 and 1/4" leak opened 44

30. FFT and power spectrum for the setup with Mic at Location 3 and 1/16” leak opened 44

31. FFT and power spectrum for the setup with Mic at Location 3 and 1/8” leak opened 45

Figure Page

32. FFT and power spectrum for the setup with Mic at Location 3 and all leaks opened 45

33. Amplitude of the sounds with different leak configurations at different locations in the test section 47

34. Amplitude of the sounds with different leak configurations at different locations in the test section 48

35. General layout of the desert gold app 51

36. Selection of are of interest 51

37. Soil survey of the area of interest 52

38. graphic view of different soil types in the area of interest 52

39. Schematic of how the person carried the GPR. The transmitter is 2 ft apart from the receiver 53

40. General velocity palette 54

41. Palette for signalling out reflectance of 35% (Gravel and concrete) 54

42. Palette for signalling out reflectance of 47% (Water in sand) 55

43. Sand box setup 55

44. Sand box with metallic pipe along the setup 56

45. Sand box with metallic pipe across the setup 56

46. Sand box with PVC pipe 57

47. Sand box with no water 57

48. Sand box with 1 litre of water 58

49. Sand box with 2 litre of water 58

Figure Page

50. Walking across the road with wall intact at first location.....58

51. Walking across the road with wall intact at second location.....60

52. Walking across the road towards the canal where the wall was broken, thicker red line on the left end indicates the water content increases as we move closer to the canal.....61

53. Walking across the road towards the canal where the wall was broken, thicker red line on the left end indicates the water content increases as we move closer to the canal 62

54. GPS tracking of our path taken.....63

55. Layout of the findings.....64

56. 3D representation of the finding.....65

57. Side view of the 3D view.....66

58. Empty pipe (2ft dia, 3 ft deep) 67

LIST OF SYMBOLS

Symbol

1. V_m = electromagnetic velocity
2. c = speed of light
3. ε_r = relative dielectric constant
4. μ_r = relative magnetic permeability
5. P = Loss factor
6. D = Depth
7. T = Time
8. R = Reflectance

CHAPTER 1

INTRODUCTION

Improved leakage finding in water distribution systems is one of the solutions that could have a hefty initial investment, but on long term basis this is going to be a very good economic investment. The use of various smart sensors to gather data and application of advanced analytics could provide crucial information on the location of leaks in the network. Specifically non destructive methods like Ground penetrating radars, and acoustic sensors can help locate primordial leaks and, so help resolve the problem while avoiding social and economic costs. In (Zhang, 1996), a review of the various pipeline inspection techniques most commonly used in WDSs systems and wastewater collection is performed. These techniques are divided into four groups:

(a) visual techniques : Closed – circuit television and sewer scanner and evaluation technology are highlighted in the first group.

(b) electromagnetic and radio frequency techniques : This group consists of magnetic flux leakage, eddy current technique, hydro scope technology (HT), rapid magnetic permeability scan (RMPS), low frequency electromagnetic field (LFEM), passive magnetic fields (PMFs), time domain ultra wideband (UWB) and ground penetrating radars

(c) acoustic and vibration techniques : This category includes sonar, vibro-acoustics, impact echo/spectral analysis of surface waves and correlator and listening sticks for leaks.

(d) other techniques : infrared thermography, continuous wave doppler sensing technique, laser surveys, broadband electromagnetics/wave impedance probe, pipe inspection real rime assessment technique (PIRAT) and the Sahara Project.

Amongst all the above mentioned techniques, the most used and efficient for locating leaks in the supply systems are those included in the acoustic and vibration technique and the ground penetrating radars. Acoustic methods detect the acoustic wave generated by the leak based on correlation analyses of the wave velocity of the sound emitted by the pipe being inspected. These methods are popularly used in metallic pipes and are most successful. So far they have not been tested successfully in non-metallic pipes (Khulief, Khalifa, Mansour, & Habib, 2012). Apart from that, GPR has been seen as a very effective non-destructive tool that favours inspection of all Water distribution systems by getting multiple readings in multiple view of plane, and the tomographically combine them to prepare 3 dimensional view of what is underground.

The need of the industry is to have a system of data collection with advanced processing and easily interpretable tool that could provide people using the technology with an “on-demand” assessment of a particular target’s properties shape, depth and extent. These days the advancement in the portable computational facilities has brought this target in close reach and hopefully the results of this thesis work will contribute towards the same. Both the leak detection method have their own advantages and disadvantages.

To compare the performance of different methods, it is necessary to define the key attributes of a leak detection system:

1. Leak sensitivity : Can small leaks be detected?

2. Location estimate capability : Is location estimate given?

3. Operational change : Can the method work if pipeline experiences operational changes e.g. throughput change, pigging?

4. Availability : Can the method monitor a pipeline continuously i.e. 24 hours a day?

5. False alarm rate : Frequency of leak alarms generated during leak-free operations.

6. Maintenance requirement : Level of technical expertise required to maintain the system.

7. Cost : Capital expenditure (CAPEX) and on going operating costs (OPEX).

The lab experiments done in this work, the lab experiments done for the acoustic sensing act as our way of proving that the method works, while also checking what are the capabilities of and limitation of the methods.

CHAPTER 2

METHODOLOGY

Acoustic sensing

Even the most simple ordinary sounds are a complex combination of individual frequency components or harmonics with broad range of intensity and frequency. Spectrograms are representations of frequency components of audio signals as a function on time and intensity. The spectrogram program, digital audio recordings (PCM format) are analysed to produce a plot of frequency vs time, with harmonic intensity represented by a variable color scale. These Spectrograms reveal various hidden structures from the audio signals and can be used to identify or classify particular sounds.

Effectiveness of these equipment depend on multiple factors that we had to look into. To compare our work we wanted to go to a flute, where different materials, size, length and thickness of the flute. Coming off it the factors we thought would contribute to finding leaks would be pipe size, type, and depth, soil type, water table level, leak type and size, pipe pressure interfering noise, and sensitivity and frequency response of the equipment. Pipe material and diameter have a significant effect on the attenuation of leak signals in the pipe. For instance leak signals travel farthest in metal pipes and are attenuated in plastic ones the most. The lager the diameter of the pipe, the larger attenuation they have, and the harder it is to detect the leak. The frequency of the leaks also depend majorly on the material and diameter, the lager diameter and the less rigid material, the lower the frequency of the leaks. Soil type and the water table level influence the strength of the leak signals at the ground surface significantly. Leak sounds are more audible on sandy soils than on clayey ones, and on an asphalt or concrete

surface than on grass. Leak signals get muffles when the pipe in below the level of water table level. The acoustical characteristics of the leaks sound depend and change with leak type and size. Some typical kinds of sounds are generated by the corrosion pits, splits, and wearing of the pipe walls and the joints(O Hunaidi, Wang, Bracken, Gambino, & Fricke, n.d.).

Generally, the larger the leak the louder will be the sound. The more sensitive and quieter the leak sensors, and the higher the signal-to-noise ratio of the signal conditioning and recording equipment, the smaller the leaks can be detected. Modern acoustic equipment incorporates signal-conditioning components such as filters and amplifiers to make leak signals stand out. Filters remove interfering noise occurring outside the predominant frequency range of leak signals. Amplifiers improve the signal-to-noise ratio and make weak leak signals audible. If the frequency response of the equipment does not extend to sufficiently low frequencies, it can miss leaks in plastic and large-diameter pipes.

Experimental Setup

Fig 1 : Test section setup where 2 Inch diameter pipe into the 4 inch pipe

Fig 2: 1/4 , 1/16 and 1/8 inch leak

Fig 3: another look at the setup

A circulating water flow rig was set up to create a model that could behave like a real pipe with leaks with water flowing through it. Two motors with variable flow rates were used to control the speed of flow going into the test section. The test section was made out of PVC pipes which went from the motors to 2 inch thickness, and then the

main test section of 4 inch diameter. The test section was then drilled and fit with 3 different sized holes and plugs, ¼” 1/16” and ⅛”. The hydrophone was inserted in the test section and connected to an audio interface to take sound recordings into the laptop. The format of the sound recordings were changed online using a free website and then put through a code in matlab that converted it through Fast Fourier Transformation. This gives us a plot between frequency and amplitude of the sound.

Fig 4 : Hydrophone, DolphinEar *PRO* Series

Fig 5 : Audio USB interface, behringer u-phoria umc22

Hydrophone Selection

A unique "Plug and Play" hydrophone for audio professionals featuring a 600 ohm balanced output that you won't find anywhere else! Low cost and rugged enough for field or studio.

Featuring a balanced output, these hydrophones are suitable for capturing high quality underwater sounds to depths of 100 meters. While Low in Cost, DolphinEar Professional Hydrophones are ruggedly designed for the real world broadcast and production environment. It provides high levels of quality audio without the need for phantom power and the problems that can cause in an aquatic environment.

DolphinEar PRO is suitable for short, medium and long term immersion applications and is available in single cable lengths to 100 meters (328 feet). They can be frozen into ice to capture the sounds of live ice skating or sporting events; submerged in chemical laden swimming pools for added realism during swimming championships; buried in the earth; or hung in mid-ocean to monitor whale and dolphin vocalizations, fish calls, or man-made noises from boats, ships, or submarines.

Data Acquisition and Analyzer Hardware

With 4 unique models to choose from, the U-PHORIA Series has the ideal interface to make your recording experience legendary. Renowned for their digital console design, Behringer's sister company MIDAS developed the world-class preamps for the UMC204, UMC202 and UMC22 interfaces”and thanks to the available +48 V phantom power, you can even use professional-grade studio condenser mics to create outstanding tracks. You take your tracks seriously, and the U-PHORIA Series respects that, providing your choice

of 96kHz resolution (UMC204/UMC202), or 48kHz resolution converters (UMC22/UM2), depending on your application. Both sampling rates offer better than CD recording quality for professional results. All U-PHORIA models provide powerful phones output with Level control and Direct Monitor select, Status, Signal and Clip LEDs, and are powered via your computers USB port so theyre ready to go wherever you go. Plus we provide free audio recording, editing and podcasting software, plus 150 instrument / effect plug-ins”just a download away at BEHRINGER.com.

- 2x2 USB audio interface for recording microphones and instruments
- Audiophile 48 kHz resolution for professional audio quality
- Compatible with popular recording software
- Streams 2 inputs / 2 outputs with ultra-low latency to your computer
- State-of-the-art, MIDAS designed Mic Preamplifier with +48 V phantom power
- Powerful Phones output with Level control and Direct Monitor select
- Status, Signal and Clip indications for perfect overview
- USB port for connection and power
- Free audio recording, editing and podcasting software plus 150 instrument/effect plug-ins "Built-like-a-tank", impact-resistant metal chassis

FFT's are usually specified by the number of input data points used in each calculation, which are always powers of two (512, 1024, 2048, etc). The frequency resolution of the spectrogram is always the digital sampling rate of the audio signal divided by the number of FFT data points. The greater the number of FFT data points, the finer the frequency resolution of the spectrogram. The maximum frequency computed by the FFT and the upper frequency limit of the spectrogram will be half the digital

sampling rate. The choice of sampling rate depends entirely on the highest frequencies in the audio signal. The rule of thumb is to use a sampling rate that is twice the highest frequency in the audio signal. That is, if you expect to have no frequency components above 11KHz, then a sampling rate of 22KHz is adequate. If you examine a spectrogram and see that all of the signal is concentrated in lower frequency components at the bottom of the display then it is a good bet that the recording was sampled at too high a rate, wasting a significant amount of memory. By varying the sampling rate and the number of FFT input data points, the frequency resolution and frequency span of the spectrogram can be chosen to best fit the audio signal of interest. Don't fall into the habit of automatically recording everything at a 44 KHz sampling rate. Lower rates often result in much better spectrogram displays. Spectrogram provides two basic modes of operation, "Analyze" and "Scan." The Analyze File and Analyze Input modes store the audio signal and spectrogram display bitmap in RAM and allow manipulation of the analysis parameters to achieve the best possible display of the data. To record a wave file using your sound card, use the Analyze Input mode for simultaneous spectrum analysis and recording. The Scan File and Scan Input modes do not store the audio signal or display bitmap and so do not allow manipulation of the analysis parameters. However, scanning of either a data file or audio input will provide a real-time high resolution display of audio data of unlimited length.

(Brodetsky & Savic, 1993) developed an approach to identify the noise of leaking gas in a pipeline and isolate this signal from the other background noise sources. Their acoustic model adopted an electric transmission line formulation instead of the standard

acoustic wave equation. This model was developed into a leak pattern-recognition system in terms of an autoregressive-moving average scheme (ARMA).

(Rocha, n.d.) introduced one of the early leak-detection techniques on the basis of acoustic measurements, wherein two pressure sensors were used for recording the leak-induced pressure waves while applying noise cancellation to eliminate the background noise. Low-frequency waves were capable of traveling the large distances between pipeline shut-off valves, without excessive damping. The change in pipeline velocity associated with the sudden appearance of a leak causes an acoustic pressure wave signal, which could be detected for small leaks, when noise cancelation was employed.

The FFT is a fast algorithm for computing the Discrete Fourier Transform if we take a 2-point DFT and 4-point DFT and generalize them to 8-point, 16-point, ….., 2^r-point, we get the FFT algorithm.

To compute the DFT of an N-point sequence using equation would take $O(N^2)$ multiplies and adds. The FFT algorithm computes the DFT using $O(N \log(N))$ multiplies and adds.

In complex notation, the time and frequency domains each contain one signal made up of N complex points. Each of these complex points is composed of two numbers, the real part and the imaginary part. For example, when we talk about complex sample X[42], it refers to the combination of ReX[42] and ImX[42]. In other words, each complex variable holds two numbers. When two complex variables are multiplied, the four individual components must be combined to form the two components of the product

The FFT operates by decomposing an N point time domain signal into N time domain signals each composed of a single point. The second step is to calculate the N frequency spectra corresponding to these N time domain signals. Lastly, the N spectra are synthesized into a single frequency spectrum.

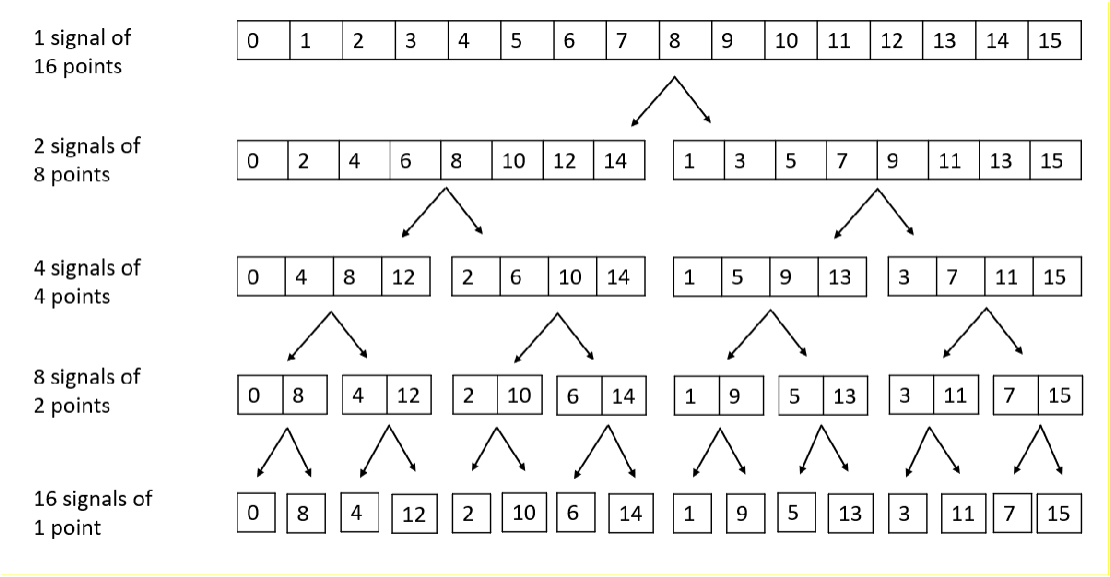

Fig 6 : Division of 1 signal of 16 points into 16 signals of 1 point

Figure 6 Shows an example of the time domain used in the FFT. In this example, a 16 point signal is decomposed through four separate stages. The first stage breaks the 16 point signal into two signals each consisting of 8 points. The second stage decomposes the data into four signals of 4 points. This pattern continues until there are N signals composed of a single point. An interlaced decomposition is used each time a signal is broken in two, that is, the signal is separated into its even and odd numbered samples. The best way to understand this is by inspecting Fig. 6 until you grasp the pattern. There are Log_2N stages required in this decomposition, i.e., a 16 point signal (2^4) requires 4

stages, a 512 point signal (2^7) requires 7 stages, a 4096 point signal (2^{12}) requires 12 stages, etc. Remember this value, Log_2N; it will be referenced many times in this chapter.

Sample numbers in normal order		Sample numbers after bit reversal	
Decimal	Binary	Decimal	Binary
0	0000	0	0000
1	0001	8	1000
2	0010	4	0100
3	0011	12	1100
4	0100	2	0010
5	0101	10	1010
6	0110	6	0110
7	0111	14	1110
8	1000	1	0001
9	1001	9	1001
10	1010	5	0101
11	1011	13	1101
12	1100	3	0011
13	1101	11	1011
14	1110	7	0111
15	1111	15	1111

Fig 7: Binary representation of the signal

Now that you understand the structure of the decomposition, it can be greatly simplified. The decomposition is nothing more than a reordering of the samples in the

signal. Figure 7 shows the rearrangement pattern required. On the left, the sample numbers of the original signal are listed along with their binary equivalents. On the right, the rearranged sample numbers are listed, also along with their binary equivalents. The important idea is that the binary numbers are the reversals of each other. For example, sample 3 (0011) is exchanged with sample number 12 (1100). Likewise, sample number 14 (1110) is swapped with sample number 7 (0111), and so forth. The FFT time domain decomposition is usually carried out by a bit reversal sorting algorithm. This involves rearranging the order of the N time domain samples by counting in binary with the bits flipped left-for-right (such as in the far right column in Fig. 7).

The next step in the FFT algorithm is to find the frequency spectra of the 1 point time domain signals. Nothing could be easier; the frequency spectrum of a 1 point signal is equal to itself. This means that nothing is required to do this step. Although there is no work involved, don't forget that each of the 1 point signals is now a frequency spectrum, and not a time domain signal.

The last step in the FFT is to combine the N frequency spectra in the exact reverse order that the time domain decomposition took place. This is where the algorithm gets messy. Unfortunately, the bit reversal shortcut is not applicable, and we must go back one stage at a time. In the first stage, 16 frequency spectra (1 point each) are synthesized into 8 frequency spectra (2 points each). In the second stage, the 8 frequency spectra (2 points each) are synthesized into 4 frequency spectra (4 points each), and so on. The last stage results in the output of the FFT, a 16 point frequency spectrum.

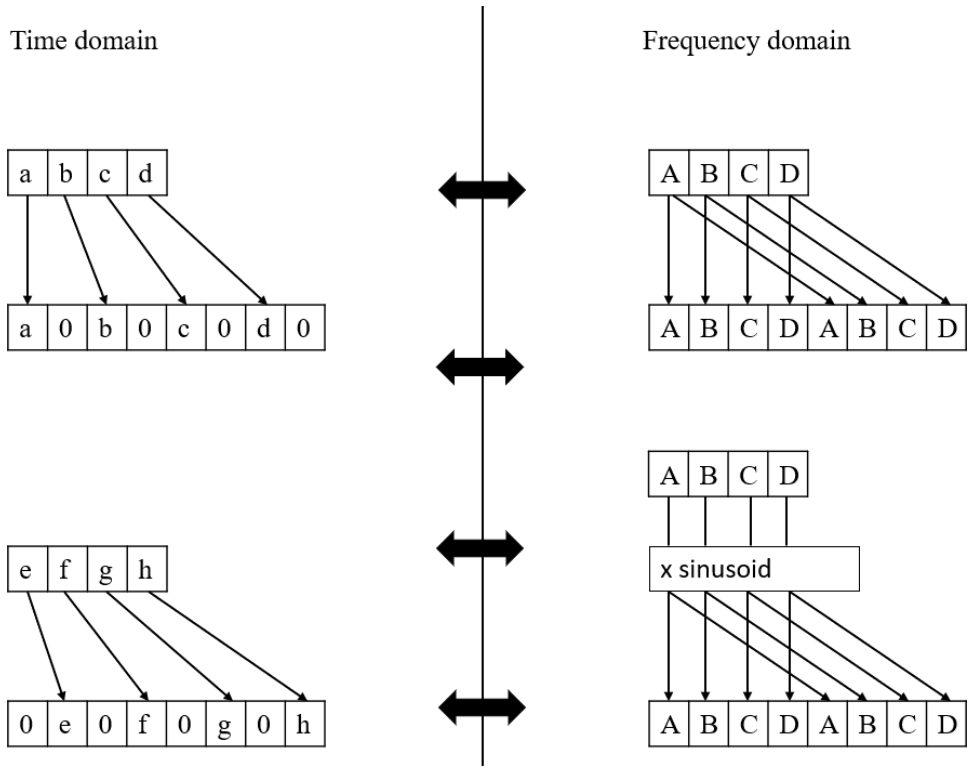

Fig 8: Functioning of the conversion from time domain to frequency domain

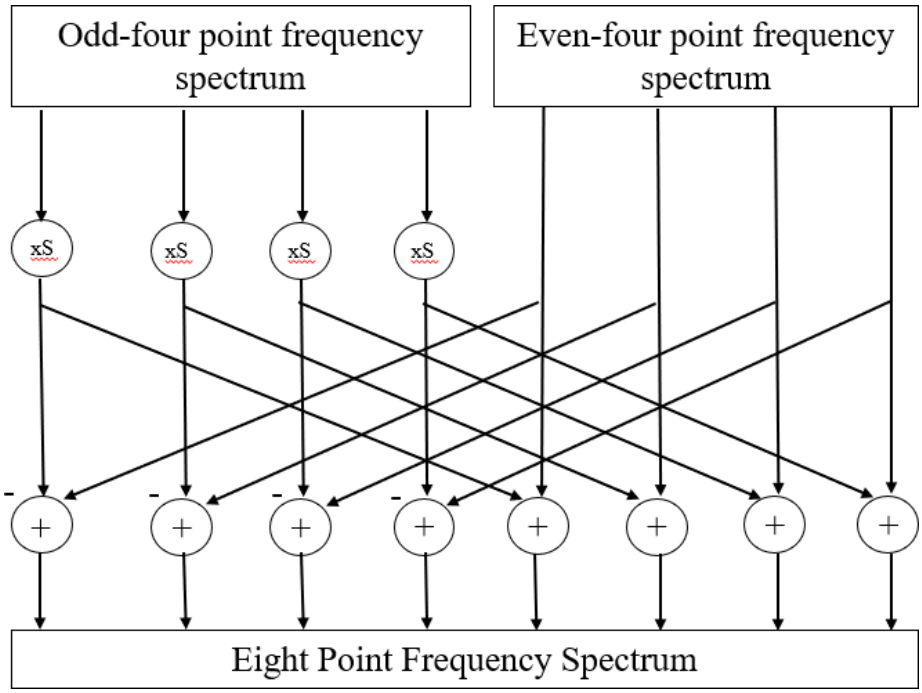

Fig 9: Mixing of the odd and even spectrum

Figure 8 shows how two frequency spectra, each composed of 4 points, are combined into a single frequency spectrum of 8 points. This synthesis must undo the interlaced decomposition done in the time domain. In other words, the frequency domain operation must correspond to the time domain procedure of combining two 4 point signals by interlacing. Consider two time domain signals, abcd and efgh. An 8 point time domain signal can be formed by two steps: dilute each 4 point signal with zeros to make it an 8 point signal, and then add the signals together. That is, abcd becomes a0b0c0d0, and efgh becomes 0e0f0g0h. Adding these two 8 point signals produces aebfcgdh. As shown in Fig. 8, diluting the time domain with zeros corresponds to a duplication of the

frequency spectrum. Therefore, the frequency spectra are combined in the FFT by duplicating them, and then adding the duplicated spectra together.

In order to match up when added, the two time domain signals are diluted with zeros in a slightly different way. In one signal, the odd points are zero, while in the other signal, the even points are zero. In other words, one of the time domain signals (0e0f0g0h in Fig. 8) is shifted to the right by one sample. This time domain shift corresponds to multiplying the spectrum by a sinusoid. To see this, recall that a shift in the time domain is equivalent to convolving the signal with a shifted delta function. This multiplies the signal's spectrum with the spectrum of the shifted delta function. The spectrum of a shifted delta function is a sinusoid. Figure 9 shows a flow diagram for combining two 4 point spectra into a single 8 point spectrum. To reduce the situation even more, notice that Fig. 9 is formed from the basic pattern in Fig 10 repeated over and over.

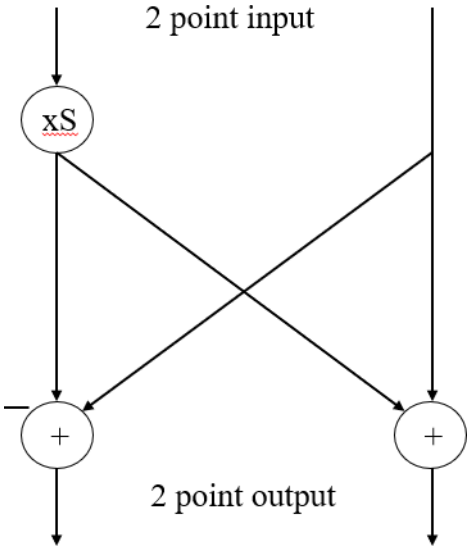

Fig 10: multiplication of the sinusoid

This simple flow diagram is called a **butterfly** due to its winged appearance. The butterfly is the basic computational element of the FFT, transforming two complex points into two other complex points.

Figure 11 shows the structure of the entire FFT. The time domain decomposition is accomplished with a bit reversal sorting algorithm. Transforming the decomposed data into the frequency domain involves nothing and therefore does not appear in the figure.

The frequency domain synthesis requires three loops. The outer loop runs through the Log_2N stages (i.e., each level in Fig. 6, starting from the bottom and moving to the top). The middle loop moves through each of the individual frequency spectra in the stage being worked on (i.e., each of the boxes on any one level in Fig. 6). The innermost loop uses the butterfly to calculate the points in each frequency spectra (i.e., looping through the samples inside any one box in Fig. 6). The overhead boxes in Fig. 11 determine the beginning and ending indexes for the loops, as well as calculating the sinusoids needed in the butterflies. Now we come to the heart of this chapter, the actual FFT programs.

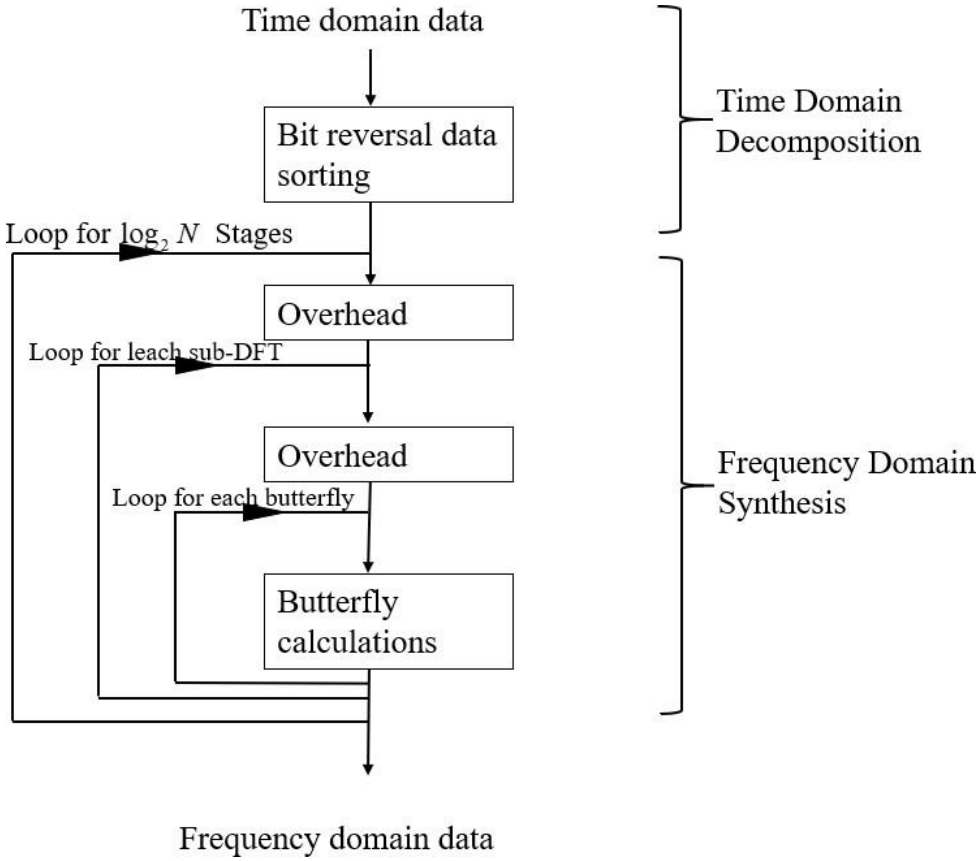

Fig 11: Conversion from time domain to frequency domain

GPR

Fig 12: Desert gold ground penetrating radar

Amongst all the geophysical methods, surveys about ground penetrating radars are coming up to be the most promising as they, in principle, lead to the “above-surface” characterization of how the pipelines have been all the while being low-cost and operator efficient. However, the large areas that usually need to be surveyed associate with utility work, and the cost and time demands of commercial data collection, it means that it is commonplace to find surveys being conducted by non-expert users and interpreted in “real time”. This is true for many geophysical techniques and for GPR in particular. In

addition, the complex nature of the near surface urban and industrial environment makes the interpretation of the utility-based geophysical surveys extremely difficult, particularly when services are over 50 years old and unmapped(Prego, Solla, Puente, & Arias, 2017).

Also, in the most recent advancements in the field of reliable microwave tomographic techniques for GPR applications have opened the way to improved imaging tools, which could provide in depth detailed information on the surveyed area when compared to standard Ground Penetrating Radar processing techniques. Under this view, we deal with the problem of detecting the water leakage from concrete pipelines and canal walls, either in its earlier stages or even when it is completely busted open, and imaging its temporal evolution from a single-fold, multi-receiver Ground Penetrating Radar survey. To achieve this target, we exploited and thoroughly analyse a specifically designed 2D tomographic approach, whose original concept and preliminary tests were reported in. In order to successfully tackle the problem at hand, in this approach the mathematical model is formulated by taking into explicit account the available knowledge on the monitored scenario, which is the locations, size and electric characteristics of the pipeline.

In the inverse scattering literature, these kinds of techniques are referred to as "distorted" wave models and are exploited to reduce the complexity and the difficulty of the problem. In this regard the use of the distorted methods and models in ground penetrating radar imaging approaches opens new and interesting perspectives. As a matter of fact, the conventional microwave tomographic techniques for ground penetrating radars applications are based on a reference scenario made of two homogenous half-spaces, that may be inadequate in several applications. Monitoring

leaking pipes in indeed one of these, as the response of the pipeline is expected to hide that of the leakage, unless this latter is large, thus precluding timely detection. In addition, the particular model consideration in this paper, in which a cooperative target is part of the reference scenario, is to our knowledge an original contribution.

To assess and analyse the proposed tomographic approach, we made use of a software that collects and represents the traces gathered by the ground penetrating radar and then by the amount of deviation from center, we calculate the reflectance which is related to the then tells us about the relation between the dielectrics between the two surfaces.

The use of ground penetrating radar as a method for locating leaks in the water distribution systems has become more widespread in recent years. In this sense, there is fieldwork, such as , performed on urban pipe sections. Like wise there is fieldwork using a combination of methods.

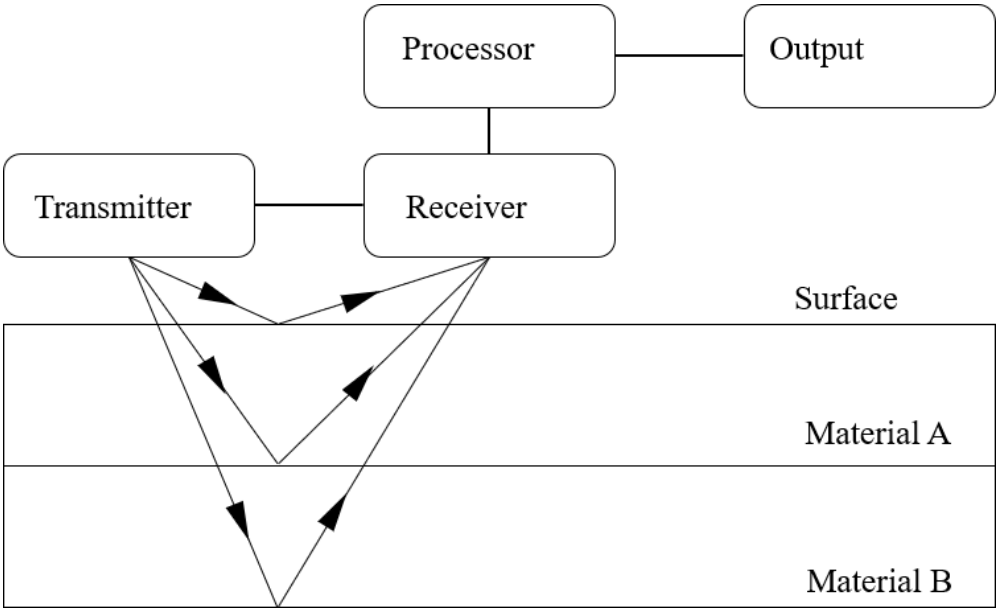

Fig 13: Working principle of the ground penetrating radar

The following general discussion may, however, help to explain the principles behind this interaction.

First, the soil reflects a large part of the radar wave at the soil surface or at inhomogeneities, which provides additional responses that may be confused with responses of real mines and therefore produce false alarms. These reflections also attenuate the transmitted wave that will reach the mine, and hence reduce the mine response(Lai, Chang, Sham, & Pang, 2016).

Another cause of attenuation of the wave on its way to the mine and back is the absorption of energy in a lossy soil. Spreading loss is also a cause for attenuation.

Another important factor is the ratio of the incident wave to the reflected wave at the mine. If the soil electromagnetic properties are close to those of a mine, the wave may

have reduced reflection when it reaches the mine, and detection at the receiving antenna might be difficult.

Figure 13 summarizes the principles of ground-penetrating radars and the wave propagation (indicated by figures). The transmitting antenna (Tx) is held at a certain distance about the ground and sends a wave to the ground that first reaches the soil surface. Since air and soil have very different electromagnetic properties a part of the wave is reflected back to the ground-penetrating radar and a part goes through the ground. This reflection at the surface is heavily dependent on the soil roughness. The energy of the transmitted wave is not emitted equally in all directions but is concentrated inside a beam. When the beam enters the soil it is refracted and becomes narrower because of the difference of electromagnetic properties between air and soil . The wave energy per unit surface is then increased, which may lead to a better detection rate and a smaller footprint. When a wave propagates in a soil that exhibits some electrical conductivity, it is gradually attenuated. The presence of localized areas with electromagnetic properties different from the surrounding soil, such as stones, roots, rocks, or cracks, can create as many reflections. When reaching a mine, part of the wave is reflected. The reflected wave then travels back through the soil. Finally the surface is reached and part of the wave propagates through the air to reach the receiving antenna (Rx) of the radar.

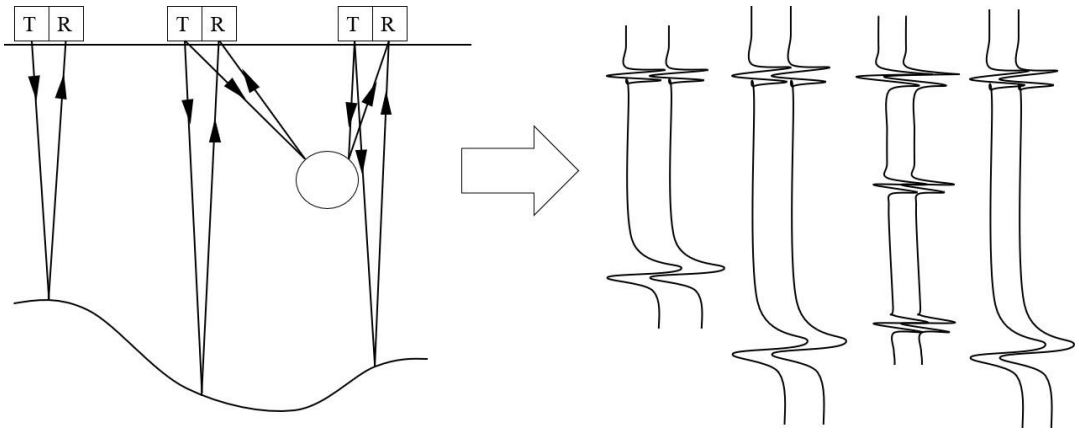

Fig 14 : Generation of traces through the GPR

The speed of electromagnetic wave in any medium depends on the speed of light in free space, the relative dielectric constant, and the relative magnetic permeability. The speed of electromagnetic wave in a material is given by :

$$V_m = \frac{c}{\sqrt{(\varepsilon_r \mu / 2)\left(\left(1+P^2\right)+1\right)}} \qquad (1)$$

Where all the parameters are same as defined in the list of parameters in the beginning.

In low-loss material, $P \approx 0$, and the speed of the electromagnetic wave is given by:

$$V_m = \frac{c}{\sqrt{\varepsilon_r}} = \frac{0.3}{\sqrt{\varepsilon_r}} m / ns \qquad (2)$$

The depth of penetration (D) can be determined by, first, calculationg the velocity of the medium, V_m , using equation (1) and (2). Second, the two way travel time (T) can be determined from the graphic representation of the GPR signals. This will allow the use of the following equation:

$$D = \frac{T.V_m}{2} \ . \qquad (3)$$

The success of the ground penetrating radar method relies on the ability of the various materials to allow or prevent the transmission of radar waves. Some materials, such as polar ice, are virtually transparent to these waves. Other materials, such as water-saturated clay and seawater, either absorb or reflect the waves to such an extent that they are virtually opaque in GPR results. The contrast in the relative dielectric constants between adjacent layers is a function of electromagnetic radiation. The greater the contrast, the greater the amount of energy reflected. The proportion of energy reflected, given by the reflection coefficient (R), is determined by the contrast in velocities, and more fundamentally, by the contrast in the relative dielectric constants of adjacent media. The amplitude reflection coefficient is given by:

$$R = \frac{V_1 - V_2}{V_1 + V_2}, \qquad (4)$$

It can also be determined by :

$$R = \frac{\sqrt{\varepsilon_2} - \sqrt{\varepsilon_1}}{\sqrt{\varepsilon_2} + \sqrt{\varepsilon_1}}, \qquad (5)$$

Where ε_1 and ε_2 are the respective relative dielectric constants (ε_r) of layers 1 and 2, respectively. Typically, ε_r increases with the depth. In all cases the magnitude of R lies in the range of ± 1 . The proportion of energy transmitted is equal to $1 - R$.

Operating frequency

Selection of the operating frequency for radar survey is not simple. There is a trade off between spatial resolution, depth of penetration and system portability. As a rule, it is better to trade off resolution for penetration. There is no use in having great

resolution if the target cannot be detected.

A simple guide is to use the following table which is based on the assumption that the spatial resolution required is about 25 % of the target depth are indicated in Table 3. There are values based on practical experience. Since every problem requires careful thought, the above values should only be used as a quick guide and not a replacement for thoughtful survey planning.

Depth (m)	Frequency (MHz)
0.5	1000
1.0	500
2.0	200
5.0	100
10	50
30	25
50	10

Table 1: Depth reached depending on soil of Arizona - dielectric 23

Table 4 provides a guide for first estimates of the velocities of common geologic materials.

Material	Typical Relative Permittivity	Electrical conductivity, mS/m	Velocity, m/ns	Attenuation, dB/m
Air	1	0	0.30	0

Distilled Water	80	0.01	0.033	0.002
Fresh Water	80	0.5	0.033	0.1
Sea Water	80	3000	0.01	1000
Dry Sand	3-5	0.01	0.15	0.001
Saturated Sand	20-30	0.1-1.0	0.06	0.03-0.3
Limestone	4-8	0.5-2	0.112	0.4-11
Shales	5-15	1-100	0.09	1-100
Silts	5-30	1-100	0.07	1-100
Clays	5-40	2-1000	0.06	1-300

Granite	4-6	0.01-1	0.13	0.01-1
Dry Salt	5-6	0.01-1	0.13	0.01-1
Ice	3-4	0.01	0.16	0.01

Table 2 : General properties of materials

Selecting sampling interval One of the parameters utilized in designing radar data acquisition is the time interval between points on a record waveform. The sampling interval is controlled by the Nyquist sampling concept and should be at most half the period of the highest frequency signal in the record. For most GPR antenna systems, the bandwidth to center frequency ratio is typically about one. What this mean is that the pulse radiated contains energy from 0.5 times the center frequency to 1.5 times the center frequency. As a result the maximum frequency is around 1.5 times the nominal center frequency of the antenna being utilized.

Selecting Antenna The plan resolution is defined by the characteristics of the antenna and signal processing employed. In general, to achieve an acceptable plan resolution requires a high gain antenna. This necessitates antenna dimensions greater than the wavelength of the lowest frequency transmitted. To achieve small antenna dimensions and high gain therefore requires the use of a high carrier frequency which generally does not penetrate the ground material sufficient depth. An important consideration when choosing equipment for any particular application is to determined correctly the exact trade-off between plan resolution, size of antenna, scope of signal processing and ability to penetrate the material.

It is important that the antenna is well isolated from the effect of the material, unless this is done, the clutter (unwanted signs whose characteristics are similar to the target) can mask the target return. Thus isolation between the transmit-receive antenna is an important parameter. Once the signal has been received it is necessary to process it from its raw state into a form more suitable for the operator. The form of processing is dependent on the type of radar, the type of target and the form of display required.
An important aspect of survey design is establishment of survey grid and co-ordinate system. The use of a standardized co-ordinate system for position recording is very important; the best data in the world useless if no one knows where they came from(Nakhkash & Mahmood-Zadeh, n.d.). Generally, surveys lines are established which run perpendicular to the trend of the features under investigation in order to reduce the number of survey lines. Line spacing is dictated by the degree of target variation in the trend direction. The selection of survey line location and orientation should be made such as to maximize target detection. All survey lines should be oriented perpendicular to the strike of the target if the target has a preferred strike direction. In attempting to cover an area to map a feature such as bedrock depth, the survey lines should be oriented perpendicular to the bedrock relie+-f and line spacing should be selected to adequately sample along-strike variations without aliasing. In situation where strike is known and the structure 2-dimensional, a very large spacing between lines can be employed. If there is no two dimensionality to the structure, then line spacing must be the same as the station spacing to assure that the ground response is not aliased. Needless to say, when Nx is a fraction in meter, a tremendous amount of data has to be collected to fully define a 3-dimensional structure.

CHAPTER 3

RESULTS

The sound recordings in the test rigs were done in controlled environment, where the water would flow in the same direction, while the hydrophone was placed in multiple location inside the pipe relative to the leaks. The three leaks of different sizes, were opened in different orientations and permutations to get all possible leak rates and see how the frequency and amplitude was affected by the leak rate. The hydrophone was also moved to various locations to see how much change does the inlet and exit make. The flow rate was also varied to see if we got any differences in the frequency spectrum, along with multiple readings over different time rates(Butterfield, Krynkin, Collins, & Beck, 2017).

The first factor we eliminated for variances and to get the most accurate reading were the sampling period of readings, and the sampling rate. After taking multiple readings at various sampling rates, we noticed that our work readings were usually between the range of 10-200 Hz, which would be good with a 4400 Hz and sampling rate of 11000 Samples per second. It would give us an accurate FFT resolution of 10.78Hz In terms of data rate, it would be 22 MegaBytes/sec.

Bandwidth (Hz)	Sample Rate (kSamples/sec)	Gbytes/Sec	FFT Resolution (Hz)
400	1	22464	0.98
800	2	43200	1.95
12800	32	691200	31.25

25600	64	1382400	62.5
51200	128	2764800	125
102000	256	5529600	250

Table 3: Sound recording parameters and quality

After the sampling rate was decided, I tried readings at 15 seconds, 30 seconds, 1 minute and 2 minutes. Taking into account multiple readings at different locations, with the same permutations of the leaks, we noticed that while there was a huge difference in the 15 sec, 30 sec and 1 minute, there was no difference between the 1 minute readings and the 2 minute readings. So to compare the results the two major factors are the amplitude of the sound and the frequency. The frequency is compared by comparing the peaks in the frequency plots, which is done by the Fast Fourier Transformation.
The way MATLAB interprets sound signals in terms of its signal strength, and its sampling rate. Once we have the the sampling rate, we specify the signal with sampling frequency of 44.1 kHz and a signal duration of 1 minute. Compute the Fourier transform of the signal, Compute the two-sided spectrum P2. Then compute the single-sided spectrum P1 based on P2 and the even-valued signal length L, Define the frequency domain F and plot the single-sided amplitude spectrum P1. On average, longer signals produce better frequency approximations. After this, the frequency spectrum was put through an overlay to reduce the noise levels. We used a box overlay at 90 percent overlay. The overlay method was welch method and was verified by generating a sound at 5000 Herts with some noises and then put through the MATLAB code[Appendix A].

As of the amplitude plot, the most reasonable way to compare the readings was to take the Root mean squared value for the plot of the signal corrupted with zero mean

random Noise. So after comparing the two values for the multiple signals, I noticed that the frequency values for the signals were not that different, but the amplitude was the factor showing variation. So, after all the time variances we concluded that for an accurate reading, and accounting for the environmental sound errors, 1-minute readings would be the best. Having longer time durations is better, but as mentioned above, the space occupied by the recordings doubles as the time increases(Osama Hunaidi & Chu, 1999).

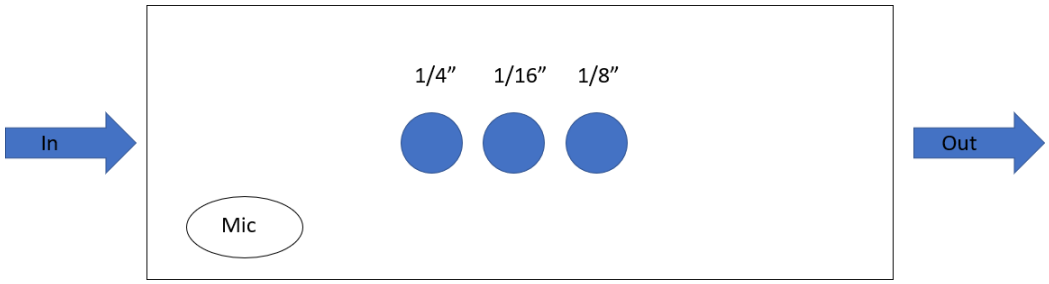

Fig 15: Schematic of the test section with hydrophone at the first location

For the first set of readings the hydrophone was placed right next to the inlet. The inlet provides a sudden increase in the flow area, with the diameter going from 2 to 4 inches resulting in some back flow. The increase in flow area would result in a reduced flow velocity according to the continuity equation, resulting in a reduction in the Reynold's number in the pipe. This would bring us closer to achieving conditions similar to our actual conditions of operation in the water distribution systems.

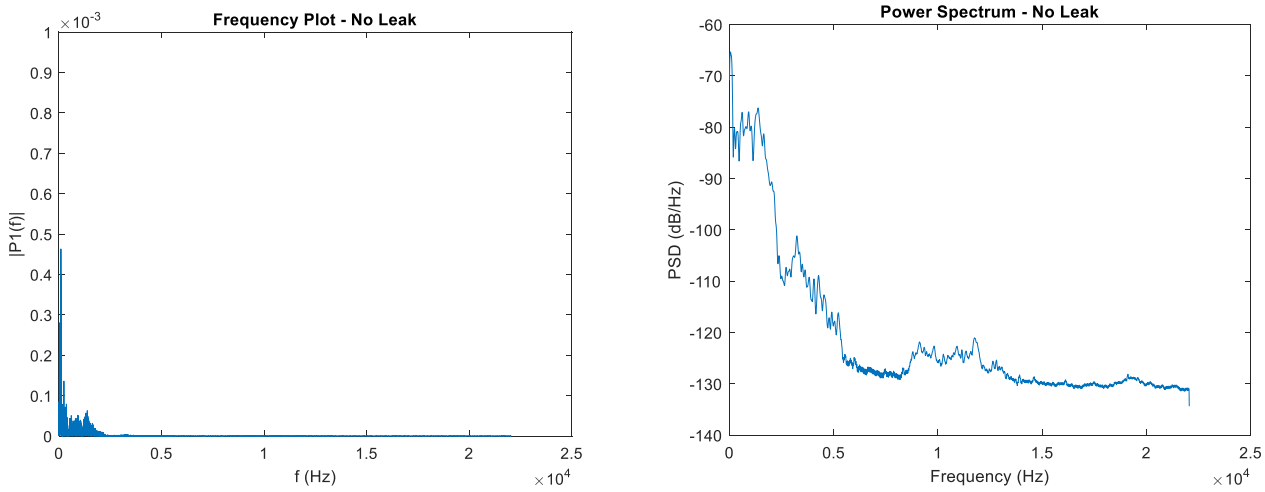

Fig 16 : FFT for the setup with Mic at Location 1 and No leak opened

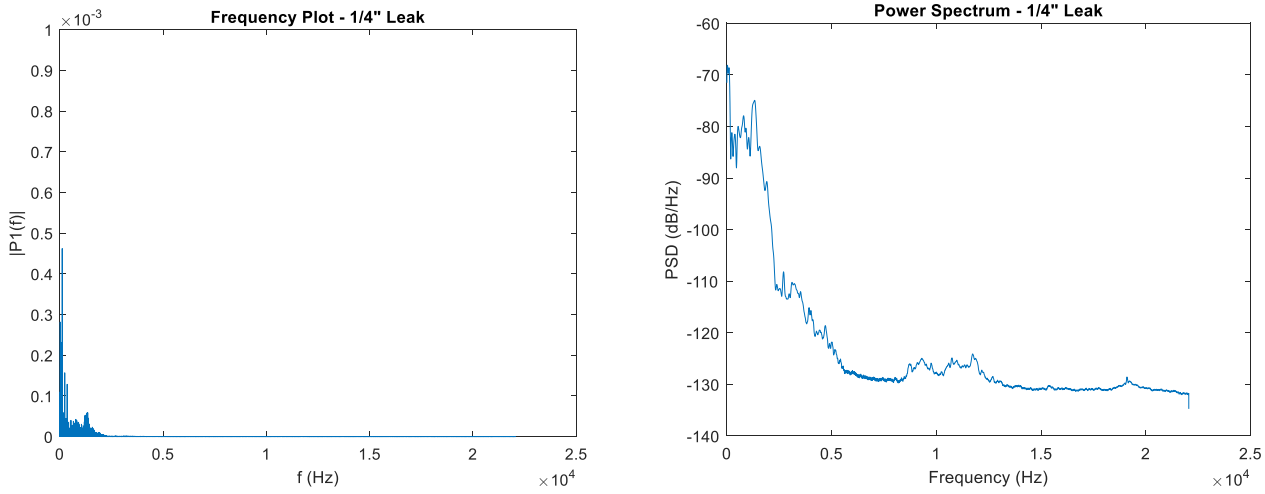

Fig 17 : FFT for the setup with Mic at Location 1 and 1/4" inch leak opened

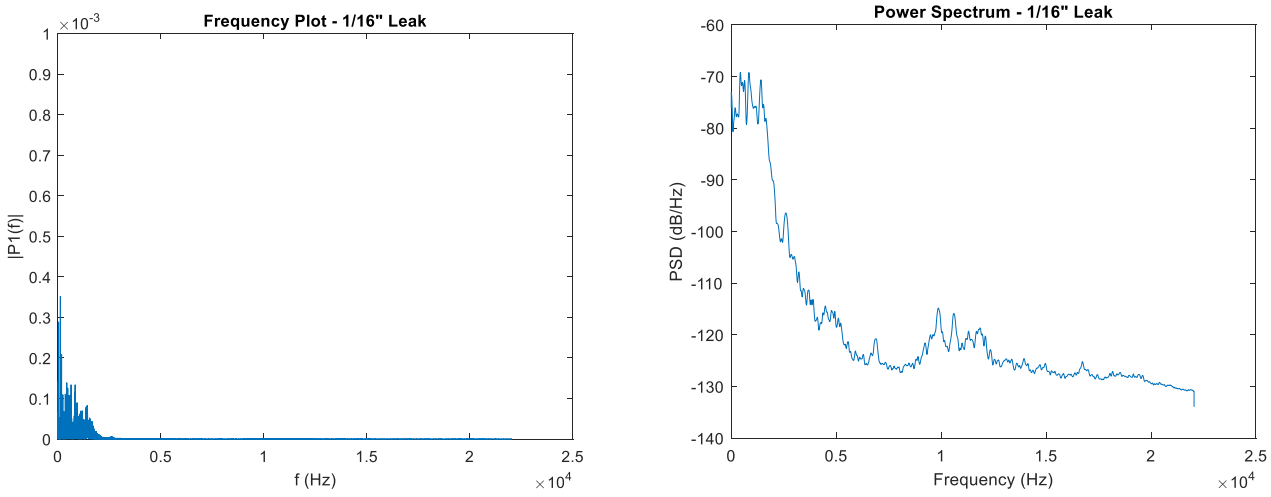

Fig 18 : FFT for the setup with Mic at Location 1 and 1/16” leak opened

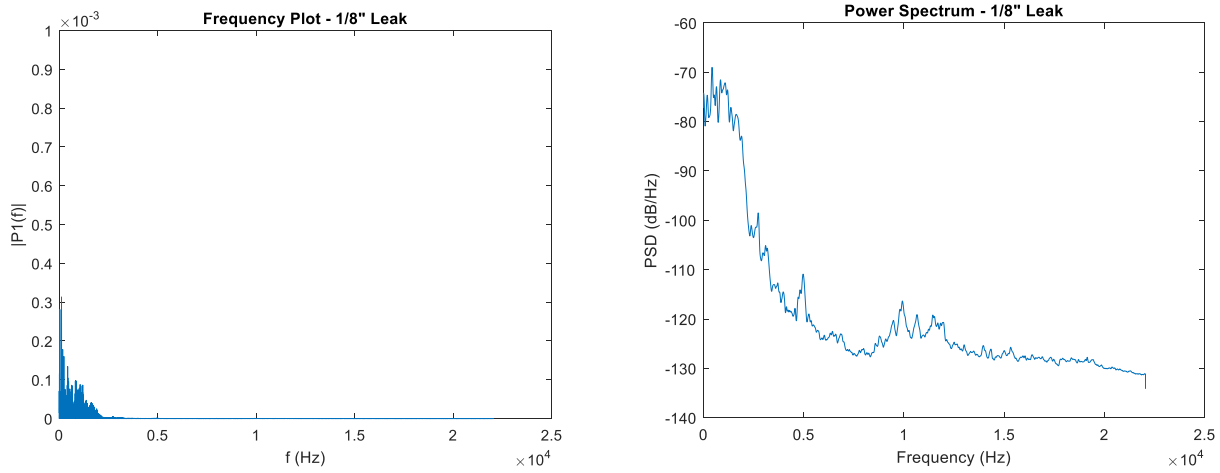

Fig 19 : FFT for the setup with Mic at Location 1 and 1/8” leak opened

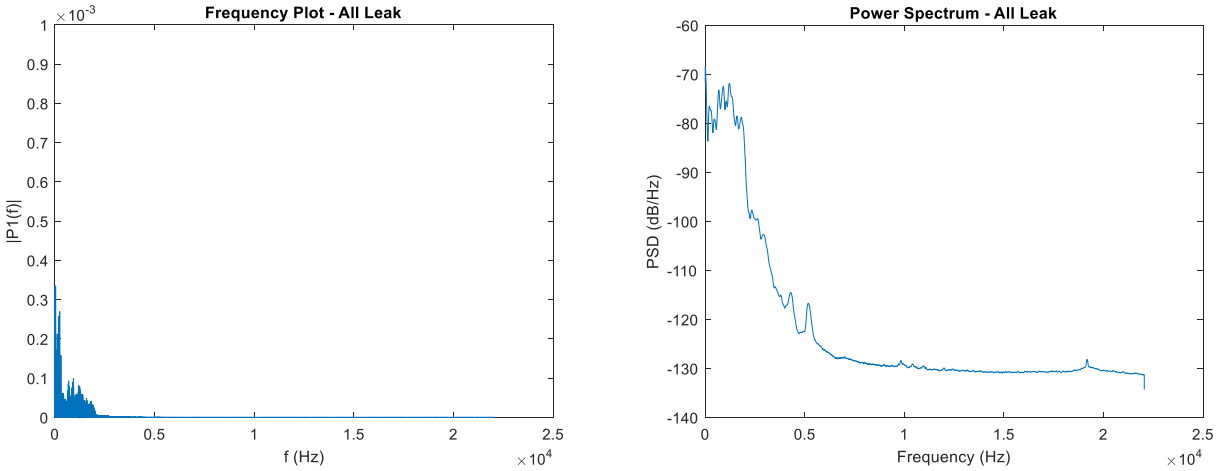

Fig 20 : FFT for the setup with Mic at Location 1 and All leaks opened

So after doing the FFT, we noticed that the frequency spectrum would peak at 90 Hz when there was no leak. The Frequency spectrum does change when we start opening the leaks. The frequency for the 1/16 inch leak, 1/8 inch leak and the 1/4 inch leak showed similar peaks, around 120Hz, while the one with no leaks showed a peak frequency at 30Hz.

When no leak was open, the power is the highest and it keeps reducing with the rate of water flowing out. Though after a certain point, somewhere between the flow rate between 1/16 inch leak and the 1/8 inch leak, and then it stays constant.

For the second part, we move the mic towards the center. The motive to do that was to notice if keeping the mic closer to the leaks would show a larger difference

between the leaks and to find a correlation between the relative positions between hydrophone and the leak. This correlation would enable us to locate the location of the leaks in the water distribution systems by not actually having to send the hydrophone inside the pipe, but taking readings at different man holes and wells already made for inspection purposes. Also, moving away from the opening, the flow would now be pretty stable, and dude to a constant velocity, the Reynold's number would be low, resulting in viscous flow.

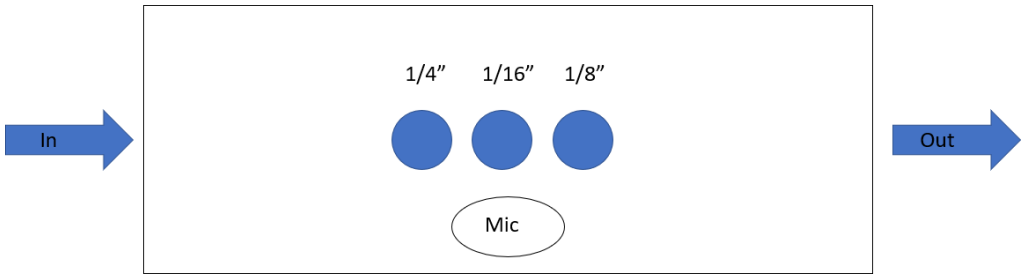

Fig 21 : Schematic of the test section with hydrophone at the second location

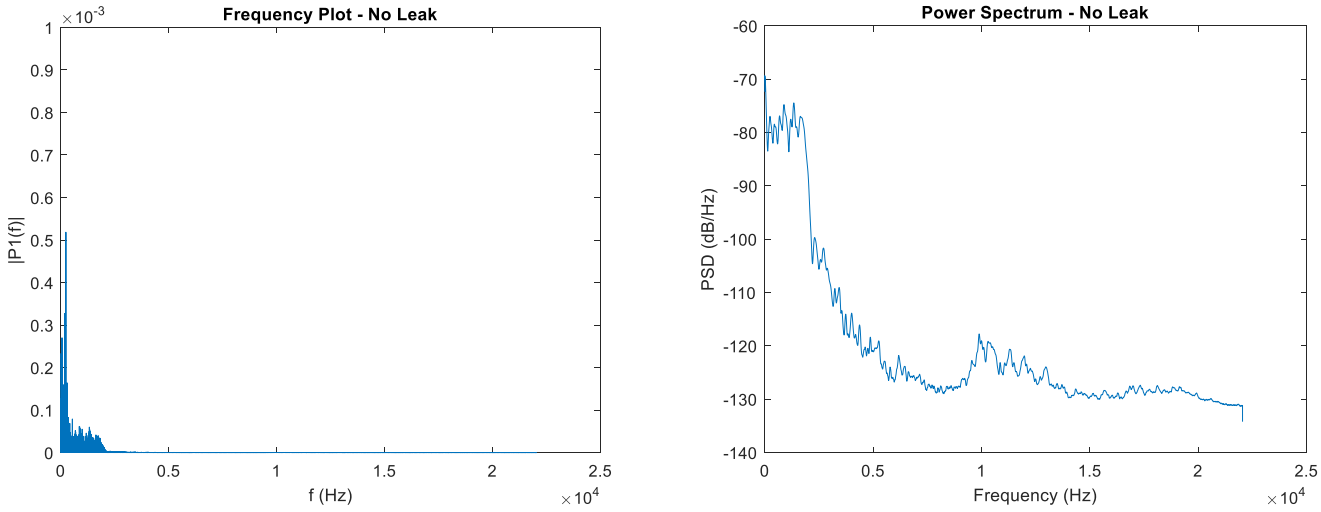

Fig 22 : FFT for the setup with Mic at Location 2 and No leak opened

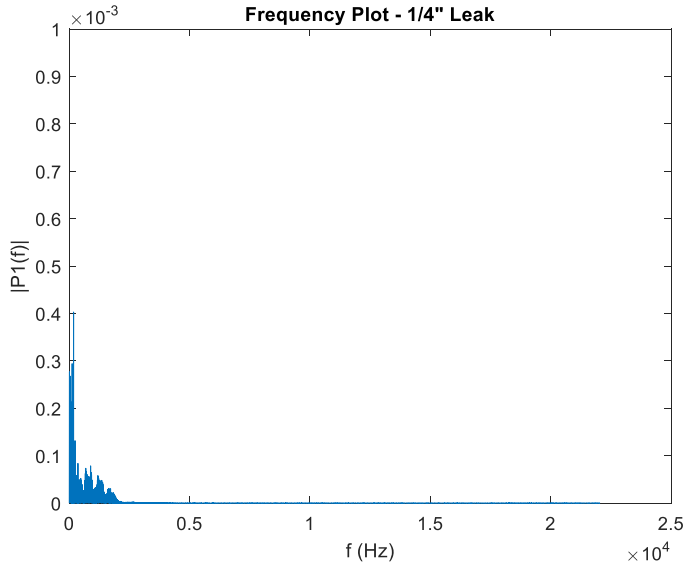

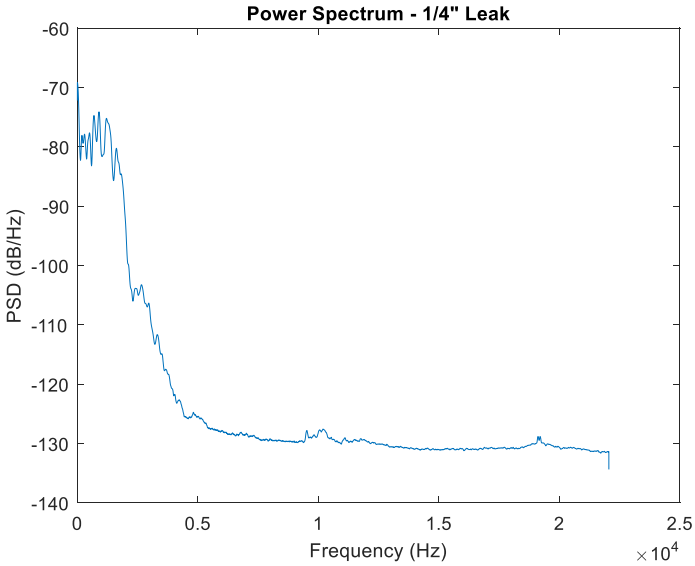

Fig 23: FFT for the setup with Mic at Location 2 and 1/4" leak opened

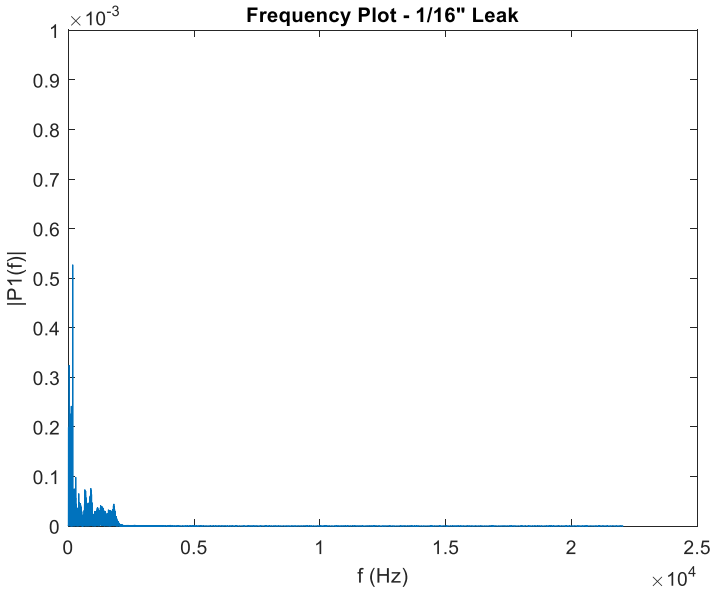

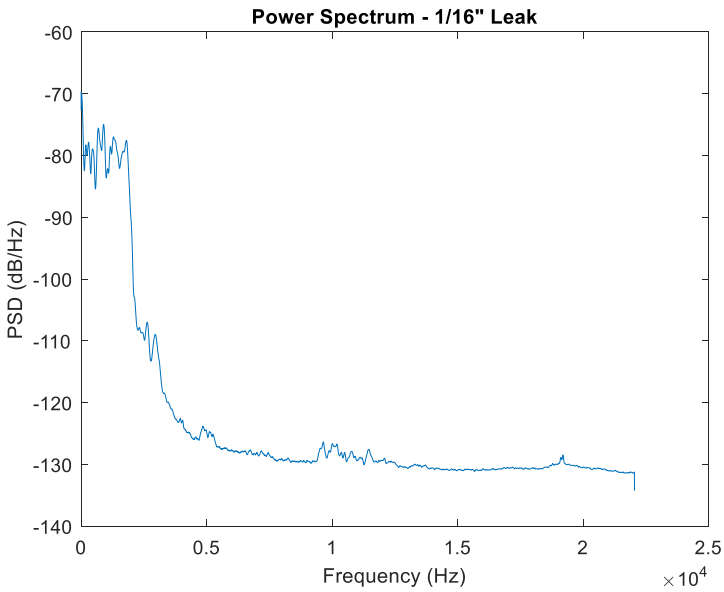

Fig 24: FFT for the setup with Mic at Location 2 and 1/16” leak opened

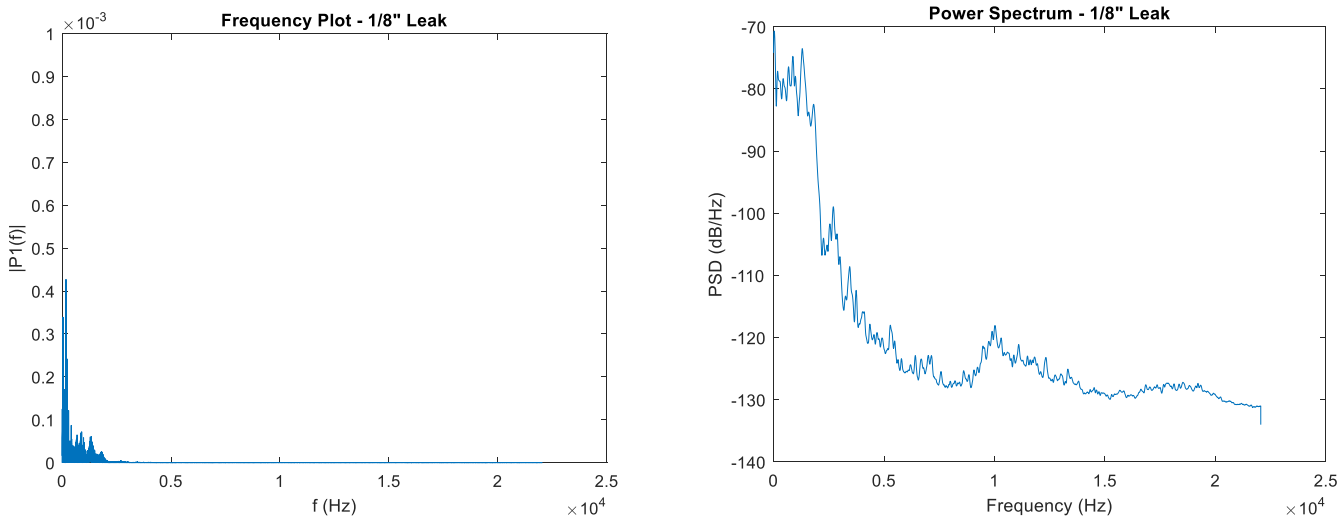

Fig 25: FFT for the setup with Mic at Location 2 and 1/8" leak opened

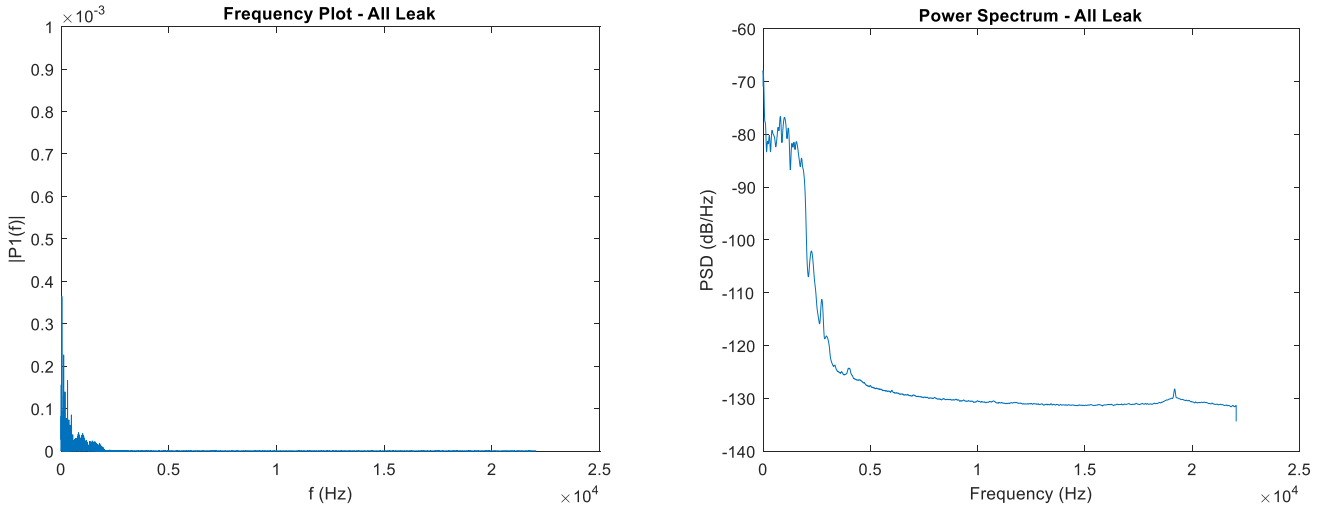

Fig 26 : FFT for the setup with Mic at Location 2 and All leaks opened

The most immediate difference that we notice when moving the hydrophone closer to the leaks, is that with every change in the leakage, there is some change in the plots. The highest frequency is displayed when none of the leaks was open at 240Hz, and

with the leaks individually open, the frequency remains constant at 180Hz. The change then is in the amplitude. The highest amplitude is shown when there is no leak, and the frequency is highest. And again like the first case, as we keep increasing the size of the leak, the amplitude of the sound keeps going down, and is the lowest the all the leaks are open.

Finally we move the hydrophone to the exit, and as we do that we notice that all the plots show similar frequency and amplitude, while the amplitudes decrease from 1/16 inch leak, to 1/4 inch leak, 1/8 inch leak and the lowest when all the leaks have been opened.

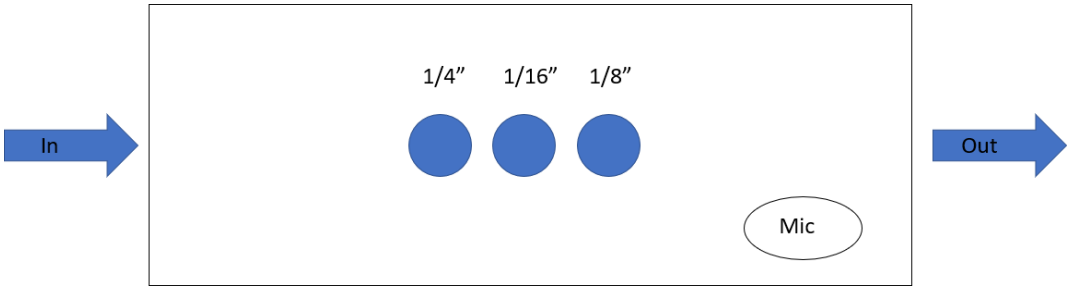

Fig 27 : Schematic of the test section with hydrophone at the third location

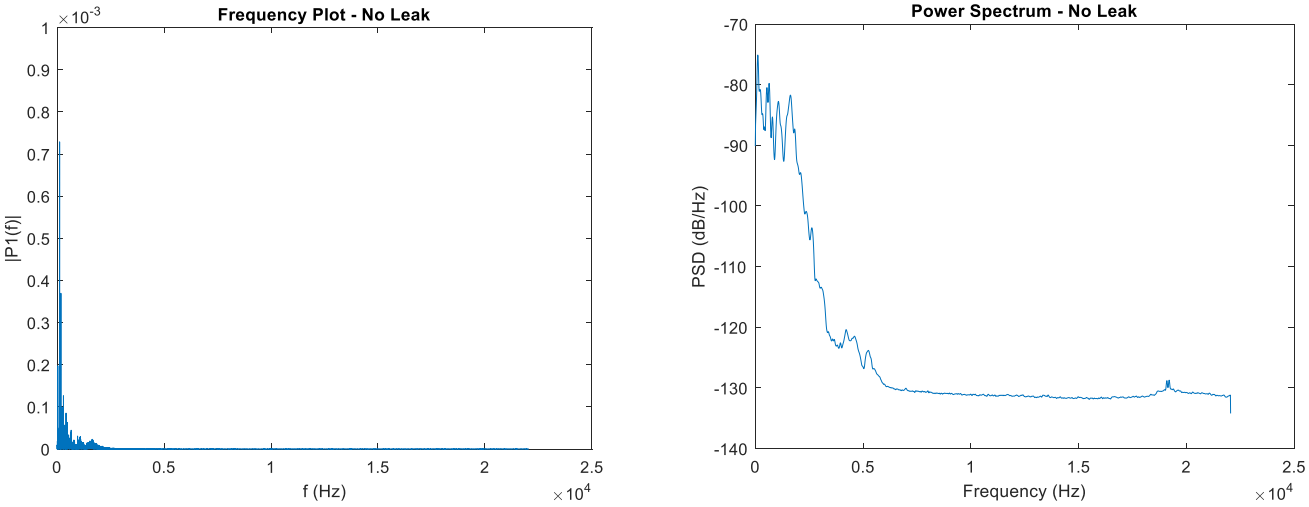

Fig 28 : FFT for the setup with Mic at Location 3 and no leak opened

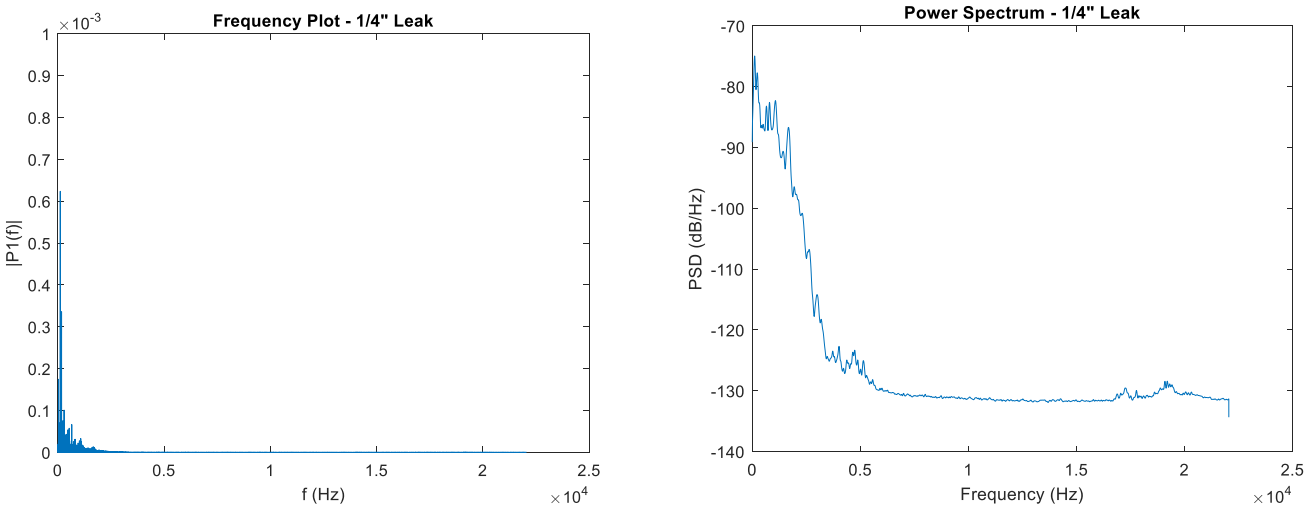

Fig 29: FFT for the setup with Mic at Location 3 and 1/4" leak opened

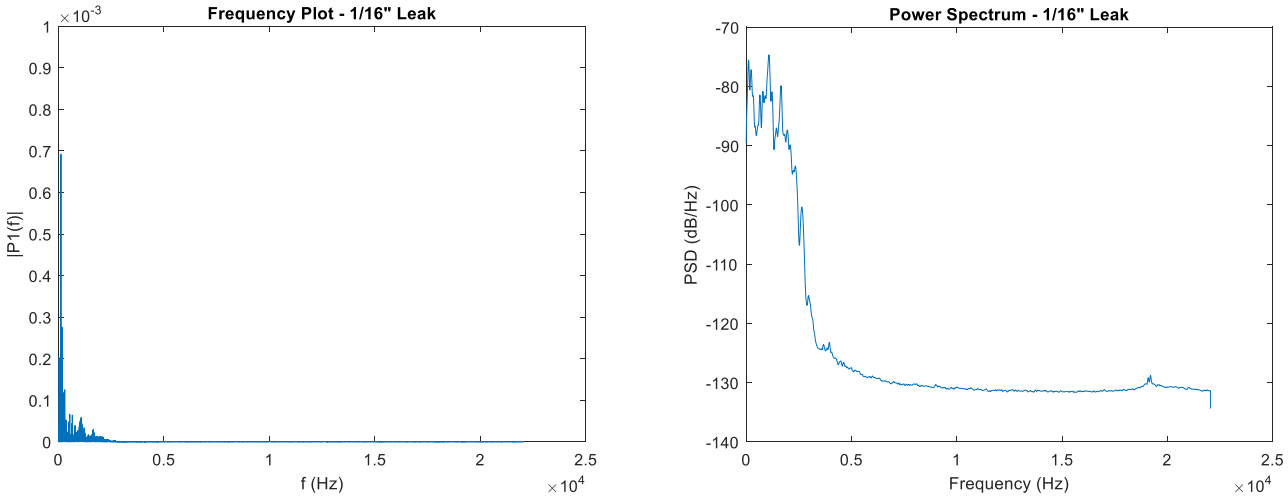

Fig 30: FFT for the setup with Mic at Location 3 and 1/16” leak opened

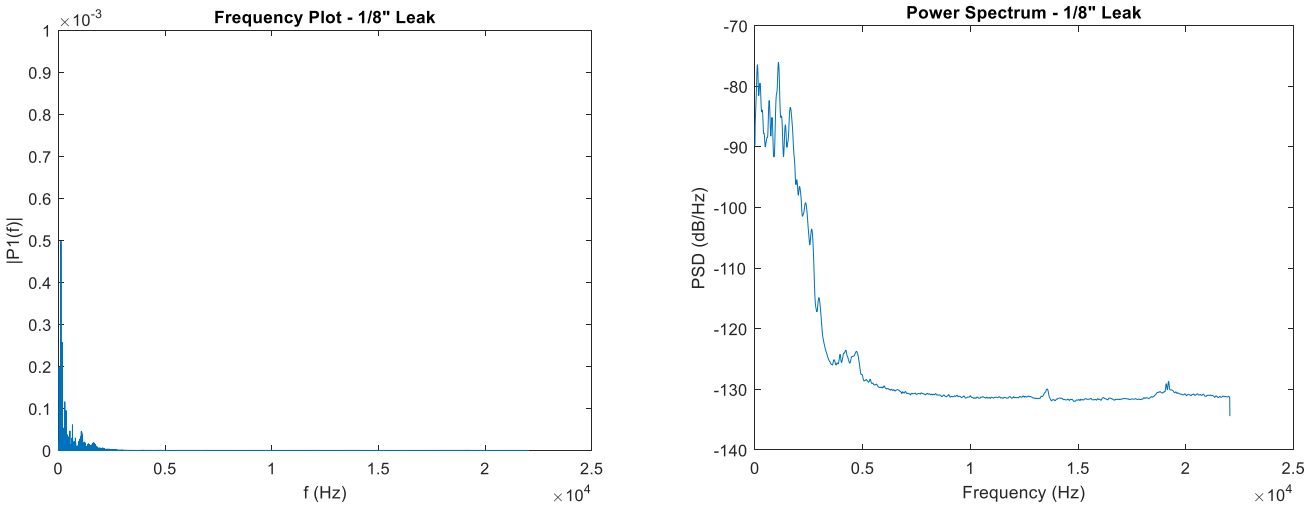

Fig 31: FFT for the setup with Mic at Location 3 and 1/8" leak opened

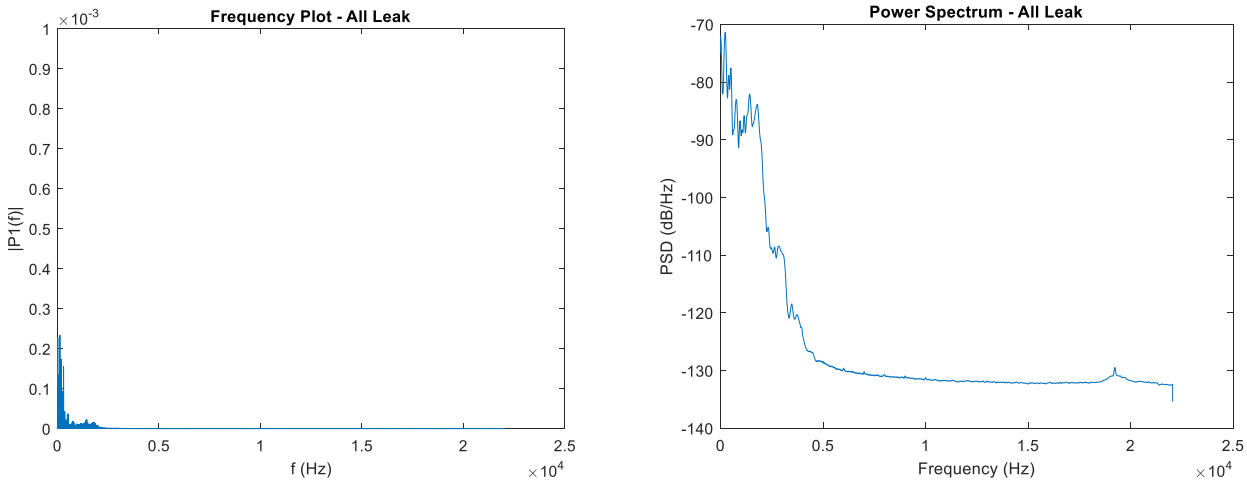

Fig 32: FFT for the setup with Mic at Location 3 and all leaks opened

From all the above results, we can see that leaks will certainly have an effect on the frequency of the flow, with every single permutation having its own specific frequency and amplitude. As seen from all the positions, the change in frequency can not be noticed from the different sizes, but that might be due to the limitations that we face because our Fast Fourier Transform Resolution restrictions. If we change in the frequencies is less than 30 Hz, we might not be seeing it on our plots. But even so, the results do depict a relation between the leaks and the frequency. A further investigation in the relation can be conducted to make sure how much it changes. A lower sampling rate could be used, but it is not possible to do so with the commercially available audio interfaces. The noise cancelling could also be improved, as while the leak does increase, the reduction in the amplitude is possibly because of the increase in noise.

The amplitude plots of the various configurations could be compared to see the affect of noise. The amplitude of the signal varied with the size of the leaks. The difference between their readings and our work was the difference between the sizes of the leaks is pretty low in our work. The other factor contributing to our work is the orientation of the hydrophone. Due to the motors being connected to the other end, the hydrophone had to be inserted into the rig from the outlet end, which might have resulted in weird movement of the hydrophone, resulting in some abrupt peaks in the amplitude plots.

The other major factor that we figured resulted in varied results was the flow rate. We connected multiple motors to increase the flow rate and checked its effects on the frequency and amplitudes. The frequency of the flow did not change with the flow rate, but this might have been due to the limitations of our resolution. The affect on the

amplitude was significant on the other hand. The amplitudes almost doubled up while showing the same behaviour in relation to the position of the hydrophone. These results show more clearly that as we move towards the end, the noise increases by a lot dure to the water running into the wall and causing more noise damping the level of sound made because of the leak.

Comparison between Average (RMS) Voltage output for low flowrate and high flow rates at different Leak settings, for 1 minute of recording.

- No leak
- 1/4” Leak Open
- 1/16” Leak Open
- 1/8” Leak Open
- All the Leaks Open at the same time

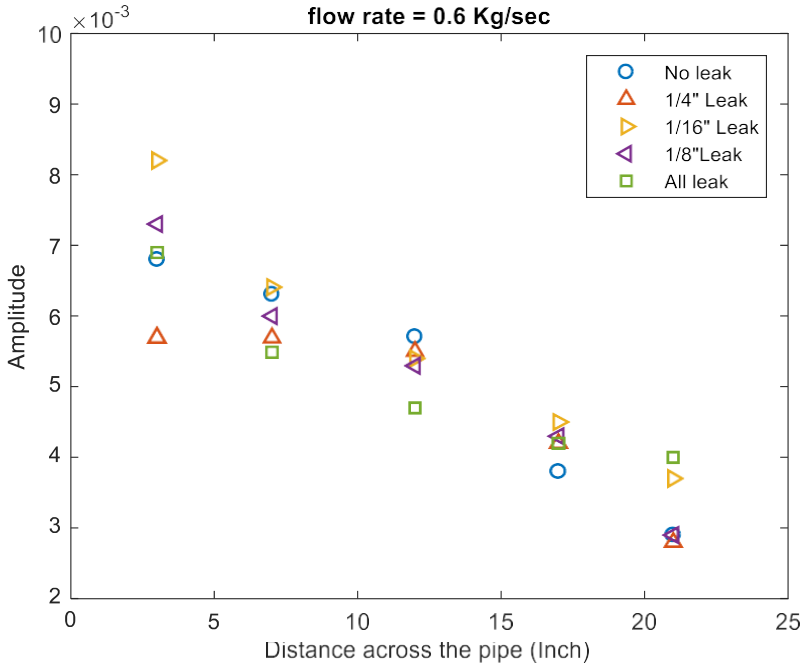

Fig 33: Amplitude of the sounds with different leak configurations at different locations in the test section

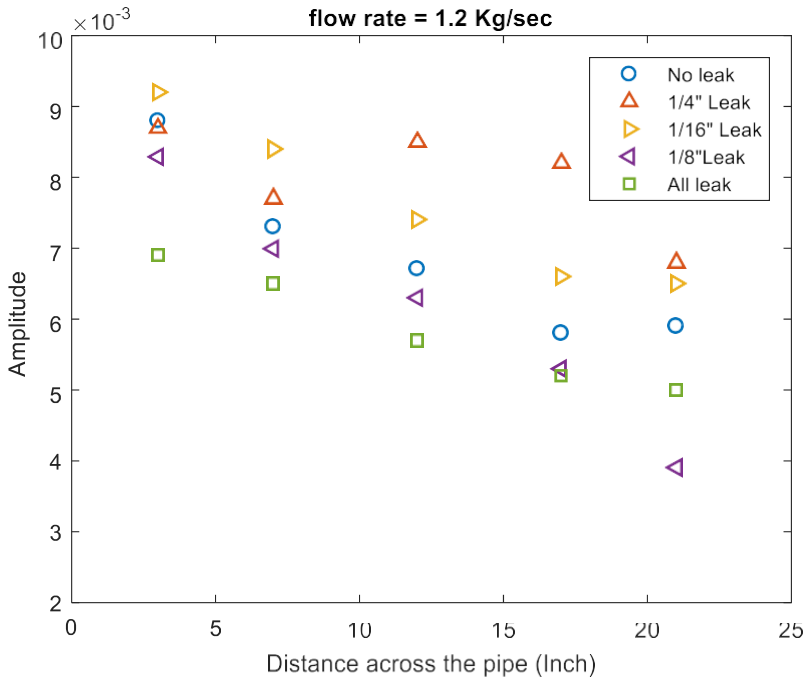

Fig 34: Amplitude of the sounds with different leak configurations at different locations in the test section

Now going back to the 7 parameters defined in the beginning, we see how well does the hydrophone work, and later compare it to the GPR.

When Leak sensitivity is considered, from the results we have seen so far, if the sensitivity of the sensor is improved, we might be able to see difference between different leaks. Based on this method there are still limitations with the leak location and the orientation of the hydrophone. We can work on a correlation between the position, amplitude, and frequency of the leak, but the noise will always be a factor that could influence the results with the hydrophone. As of the Operational changes, the hydrophone should easily be able to work while the pipeline goes through different changes.

As of now, the method we are using would not be able to give real time readings, but a method could be worked on where the sound recording's are being converted into

frequency and amplitude plots in real time so that we can see if the frequency or the amplitude changes. A major change in either would indicate a difference in the surface of the piping indicating a leak. Moreover, if multiple hydrophones are present we could compare their location with the frequency and amplitude to see if something between them is changing. Major changes in frequency or amplitude could be caused because of random objects flowing in the water distribution system, but that would not be long term. The only false alatms that could be caused would be because of different particles being stuck on the wall or because of the materials flowing through the water. If the Water distribution system has pipes of higher diameter, the flowrate or frequency would depend on how the flow changes, which would not happen until permanent changes are made to the water distribution system. The maintenance on the system would not be too high, as once the hydrophone has been installed, the only maintanenec cost would be to replace one when it totally stops working, or when there is too much sediment on the surface of the hydrophone. As of the cost, the initial investment would be pretty high depending on the distance of the sensors from the station.

The major investement in the whike system, wouls be to develop a mechanism where the signal is being convereted into frequency and amplitude plots. Thoguth it would be compliavcted,it would depend on the sampling time we use for the readings. If we reduce the time, we could be getting near immediate results for the fft, but those results would vary a lot in their accuracy about the amplitude, as any difference in the flow conditions would result in changes in the readings, as longer readings result in a larger time to be averaged upon.

GPR

For the Ground penetrating radar, we started with primary tests around the Arizona State University Tempe campus. From the soil properties found on websoilsurvey.sc.egov.usda.gov, we can use the value of the dielectric constant of the soil and input it in the desert gold program, that lets us choose the type of soil. Once we do that, we choose the type of antenna that we will be using, and based on these two parameters our maximum depth is calculated by the software. As much as higher depths are good, the results at the bottom most part are usually not the most reliable as noise distorts the waves. In interpreting the radar data one usually searches for anomalies such as hyperbolic reflections, irregularities in largely uniform reflection patterns, and changes in the frequency of the signals. Hyperbolic reflections are caused by point reflectors in the ground such as pipes, rocks, voids etc. Irregularities in largely uniform reflection patterns are usually caused by disturbances to the natural sedimentation of soils as a result of construction activities. Changes in the frequency of the radar signals are caused by changes in the dielectric properties of the transmitting medium.

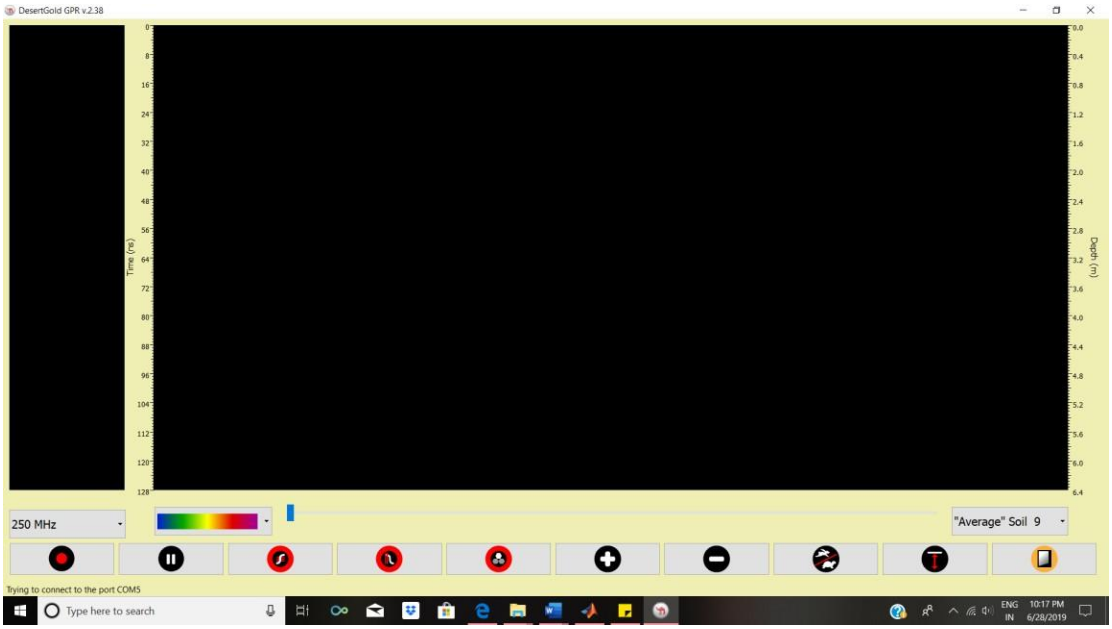

Fig 35: General layout of the desert gold app

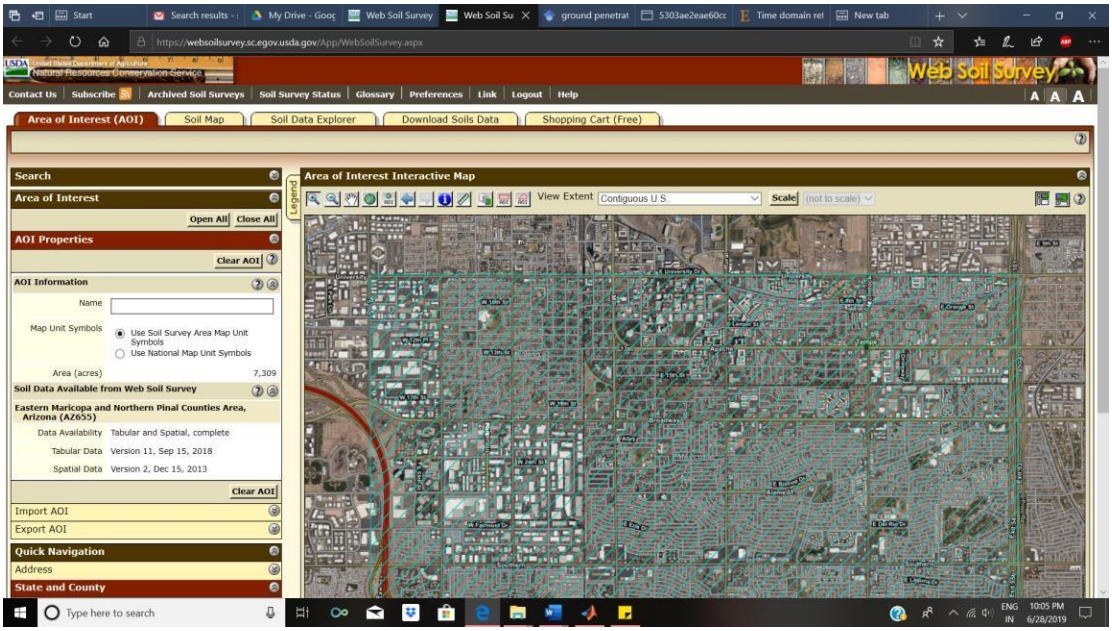

Fig 36: Selection of are of interest

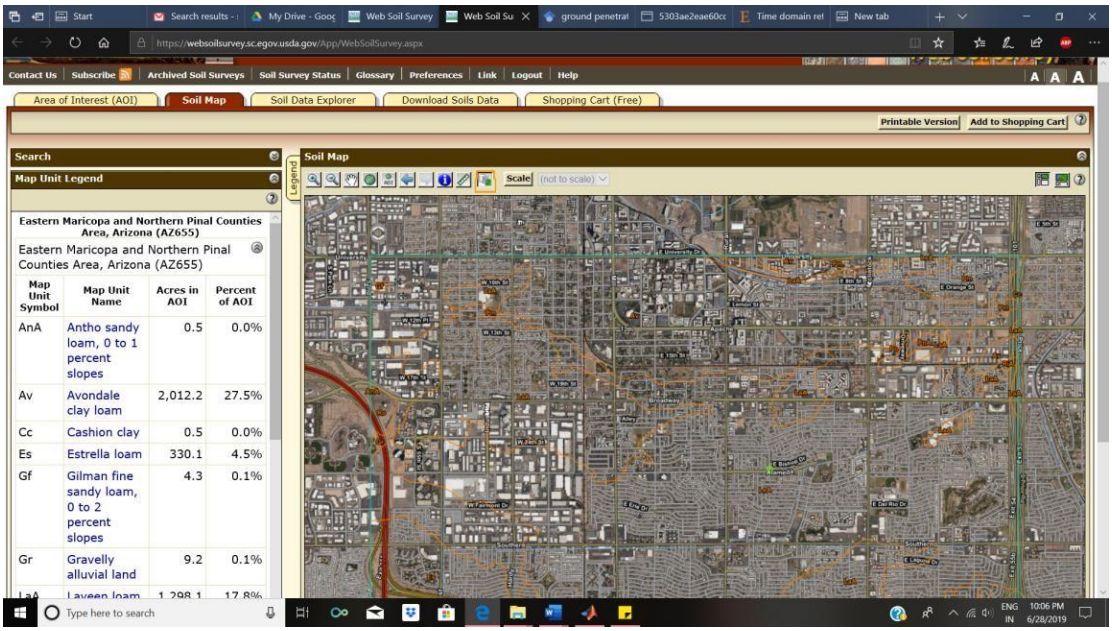

Fig 37: Soil survey of the area of interest

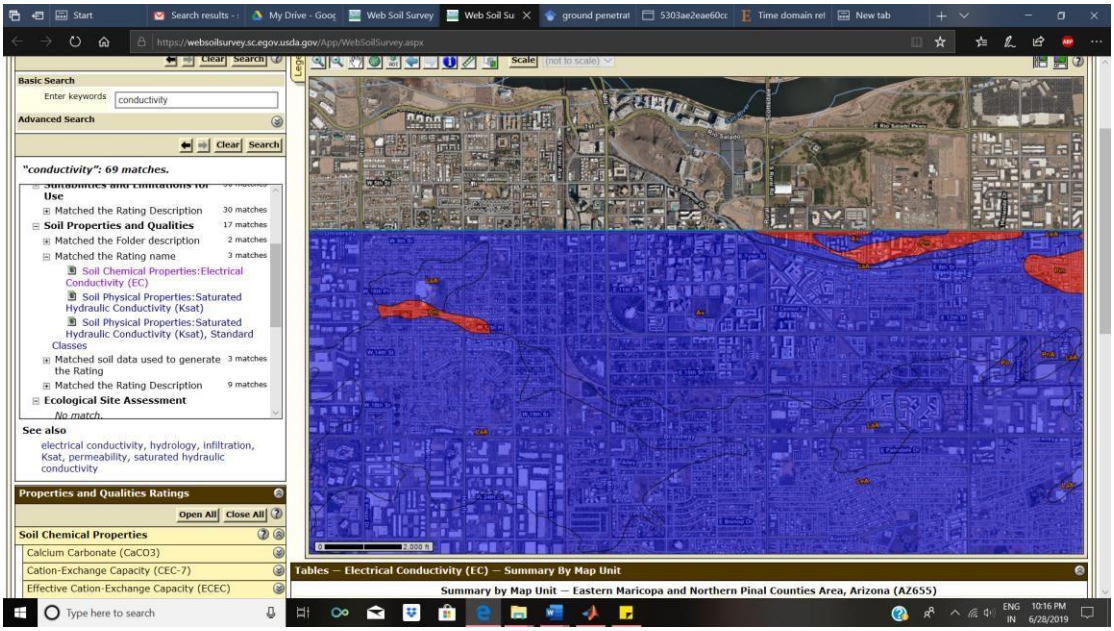

Fig 38: graphic vie of different soil types in the area of interest

The software “desert gold” allows us to change a lot of these parameters according to our need and test conditions. Accordingly, the initial tests gave us a good understanding of how to use these settings depending on where we are using the radar. A

major result we realised was that the radar we are using reacts abruptly around electrical lines, with strong electromagnetic signals.

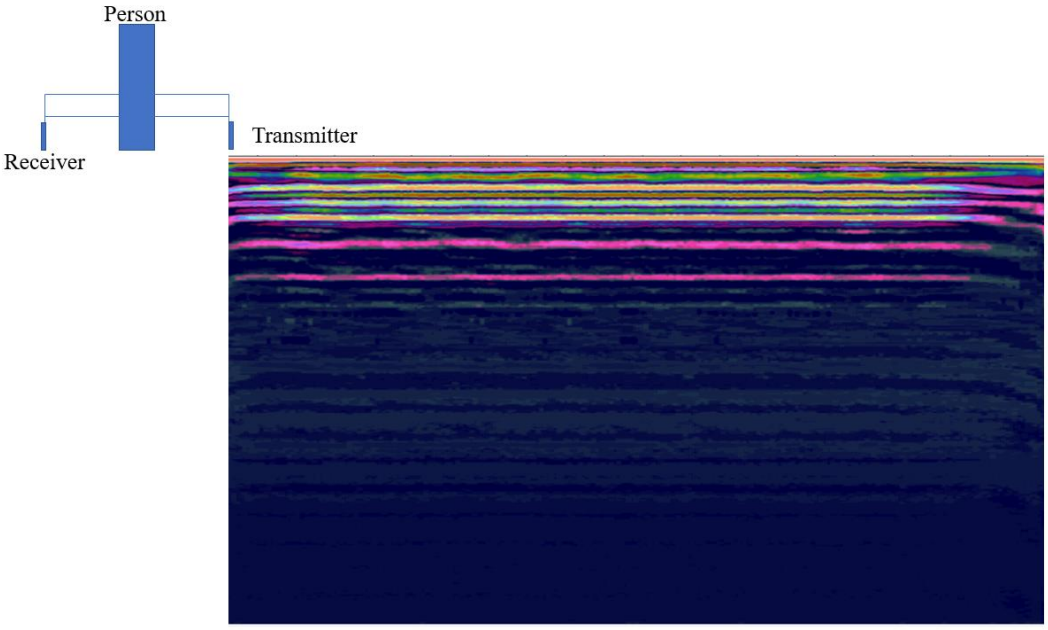

Fig 39: Schematic of how the person carried the GPR. The transmitter is 2 ft apart from the receiver.

After that, we started experimenting with the free software seisee, which lets us read and post process the seismic readings that the radar saves. In the software we can manipulate the palette according to what we need to find. Some sample palettes are displayed in figures , and , but the values of the reflectivity will depend on the di-electric of the medium, as defined in equation.

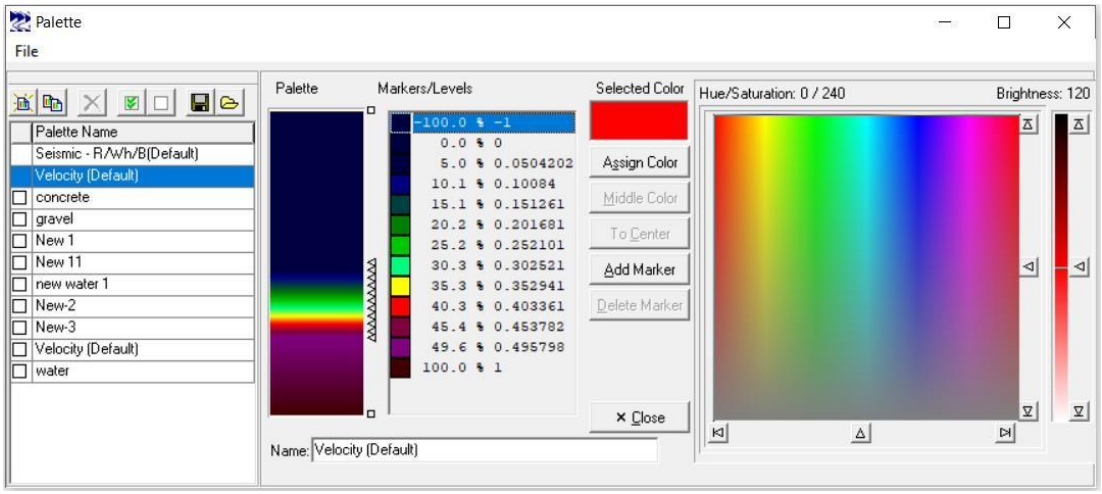

Fig 40: General velocity palette

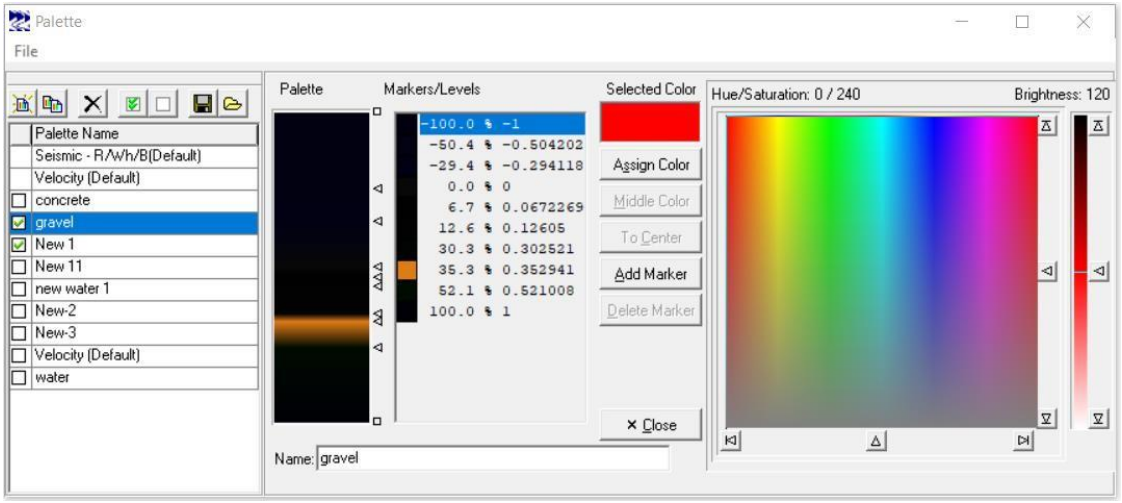

Fig 41: Palette for signalling out reflectance of 35% (Gravel and concrete)

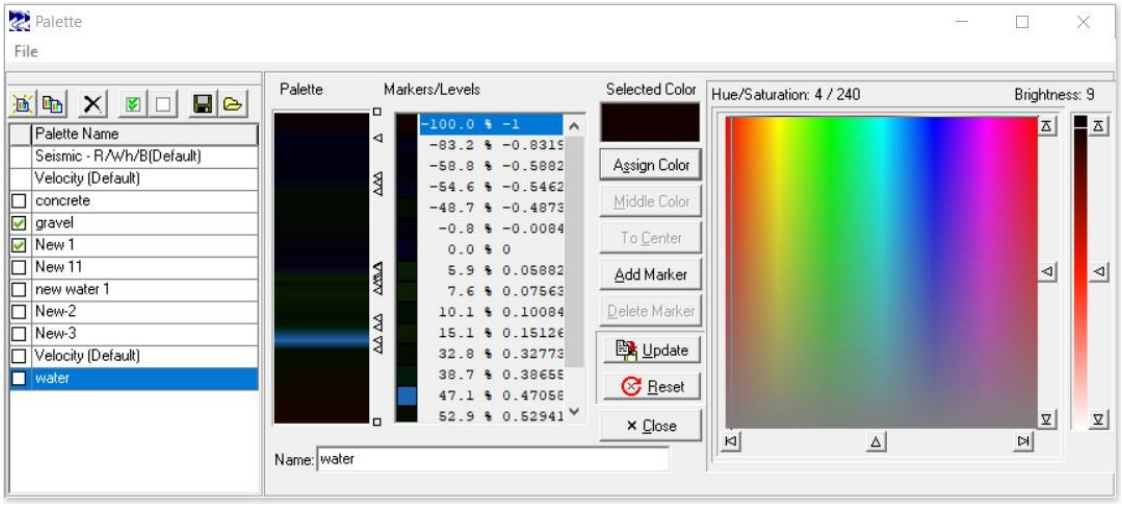

Fig 42: Palette for signalling out reflectance of 47% (Water in sand)

Fig 43: Sand box inside the lab

After this, to have a more controlled environment, we created a setup in the lab where we filled a tub of volume, with sand and silt, and buried different objects inside which included empty plastic bottles, water filled plastic bottles, metallic pipes, and pvc pipes. The results of those tests are shown in figures 44, 45, 46 and 47. The differences in these results are not very clear, but a difference can be seen. Due to the thickness of the

metallic pipes and the PVC pipe being small, it doesn't really show on the GPR, but what we can see is a slight faded out region (Marked in red) showing air inside the pipes.

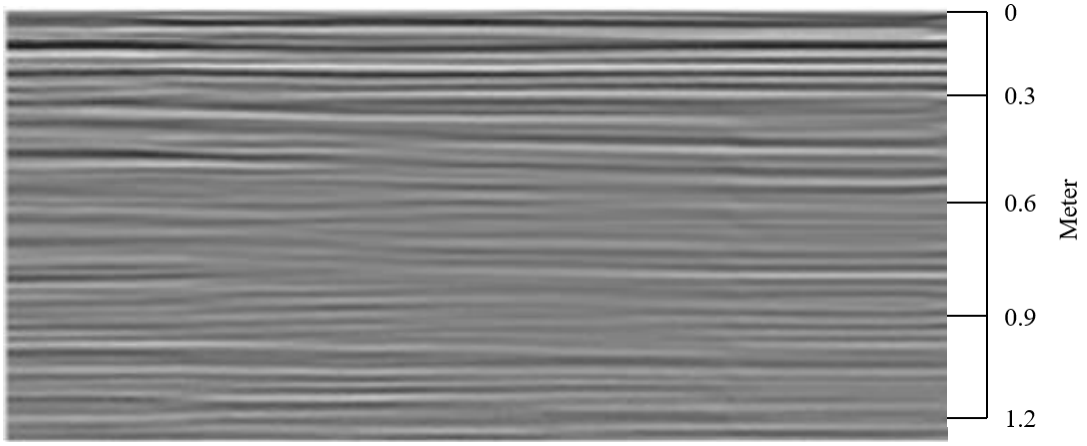

Fig 44: Sand box setup

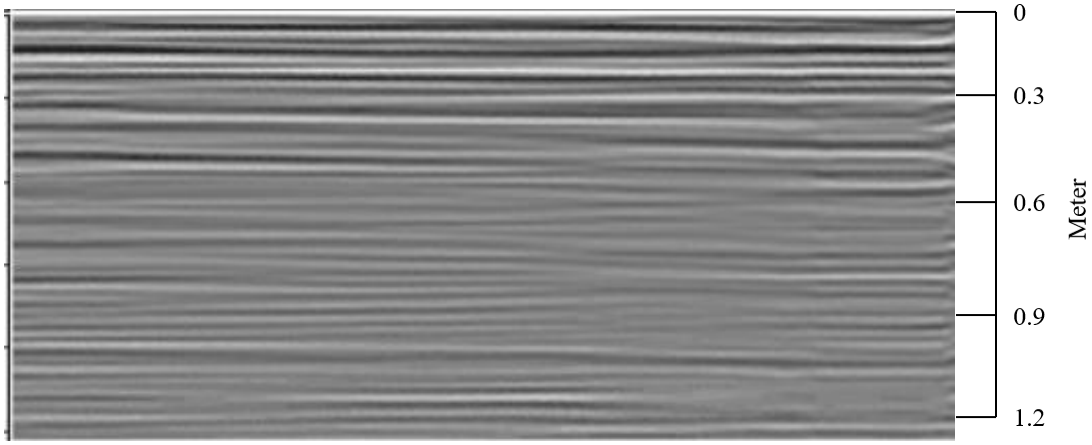

Fig 45: Sand box with metallic pipe along the setup

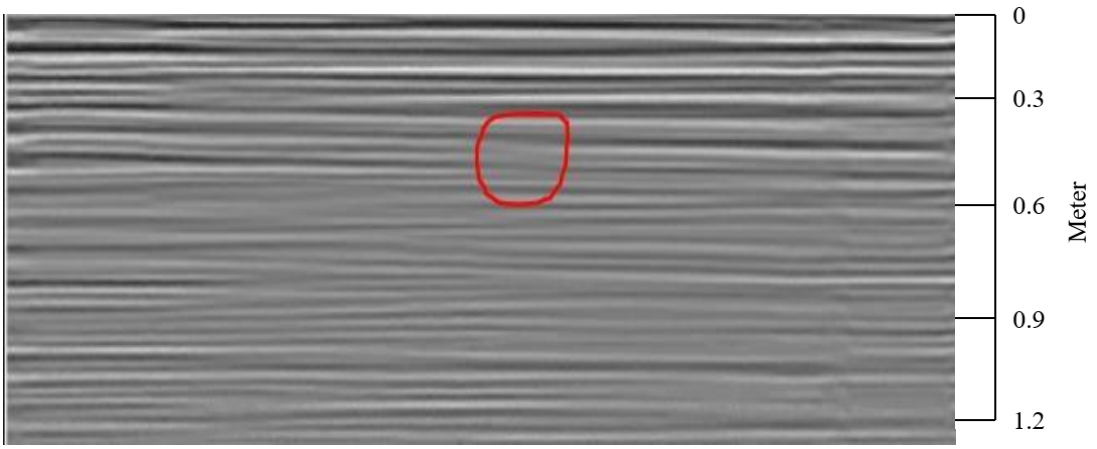

Fig 46: Sand box with metallic pipe across the setup

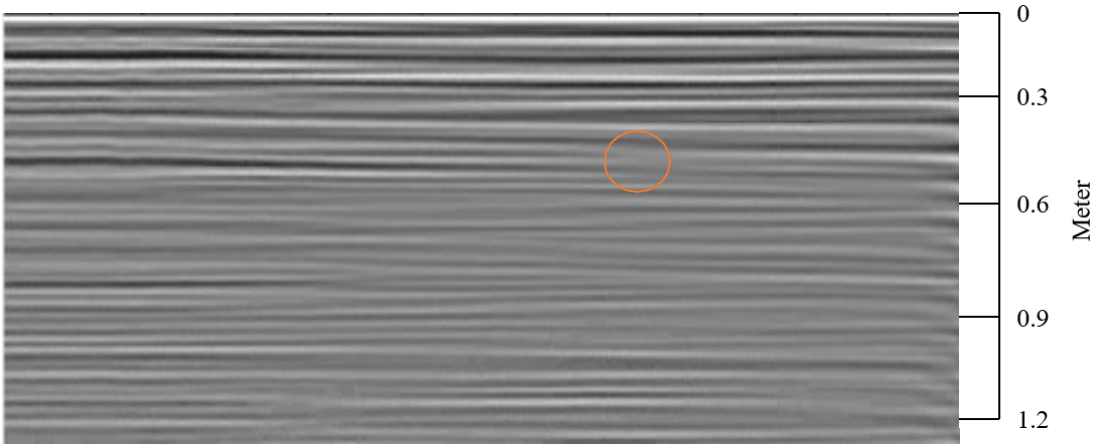

Fig 47: Sand box with PVC pipe

After that we filled up the sand box with water. Fig 47 shows the results without any object or water in the box. Fig 48 is the result with 1 liter of water, and Fig 49 with 2 litre of water close to 0.6 meters. We can see some dark maroon patches loosing their strength.

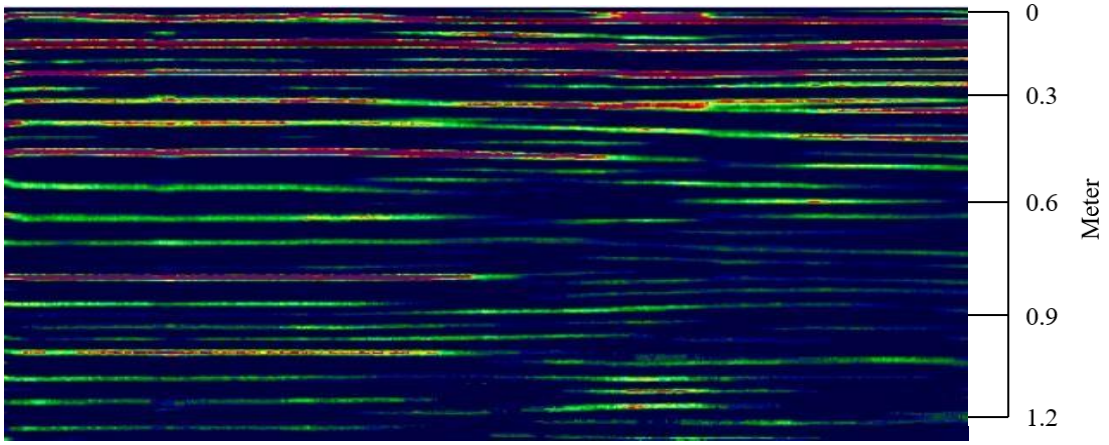

Fig 48: Sand box with no water

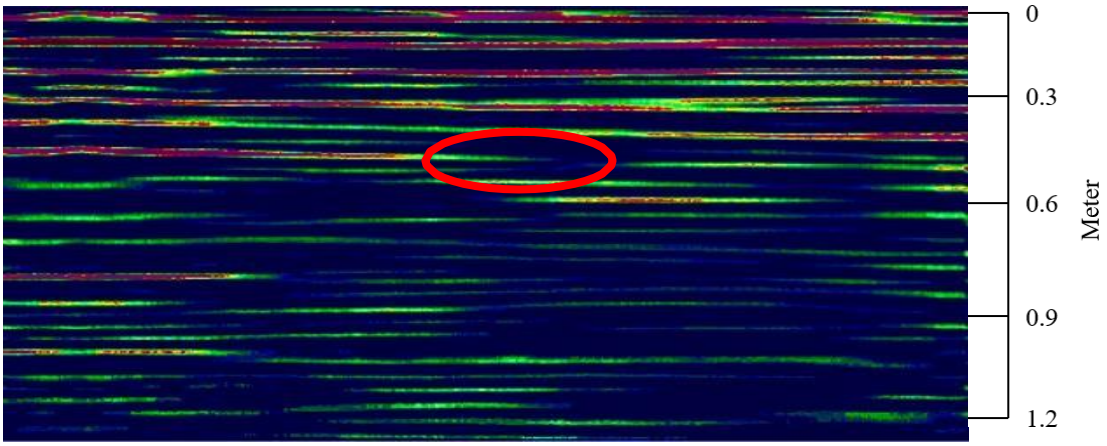

Fig 49: sand box with 1 litre of water

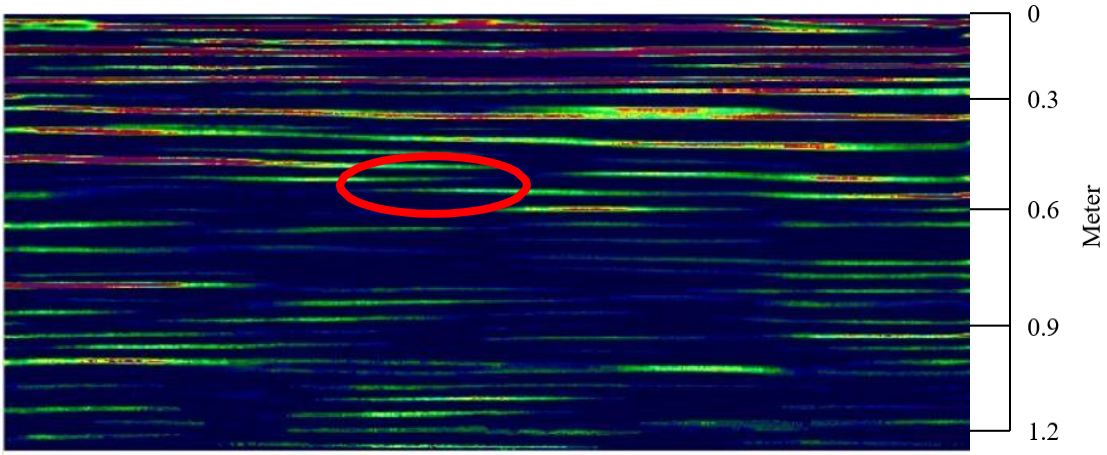

Fig 50: sand box with 2 litre of water

After this we went to a canal with broken walls near Guadalupe to get some readings. Fig 51 and 52 were taken at two different points with no breakage in the wall of the canal. As we can see both the readings have long straight lines as the results, indicating no major changes in their conditions. Fig 53 and Fig 54 are the respective reading next to the places where the wall was broken. In both the figures the dark colors are fading as we walk away from the canal. This indicates that the soil is absorbing more water close to the canal and it dissipates as we move farther away from it.

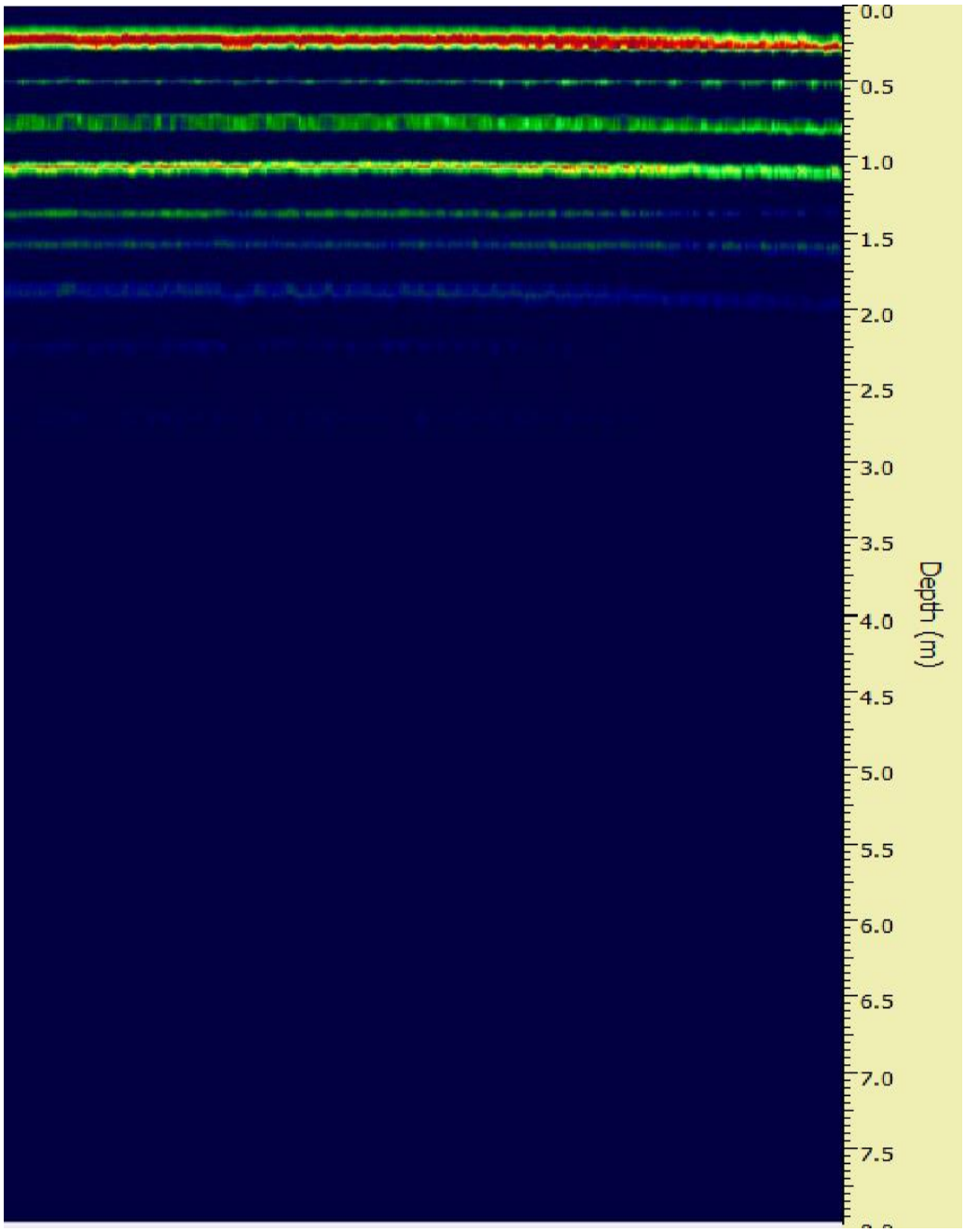

Fig 51: Walking across the road with wall intact at first location

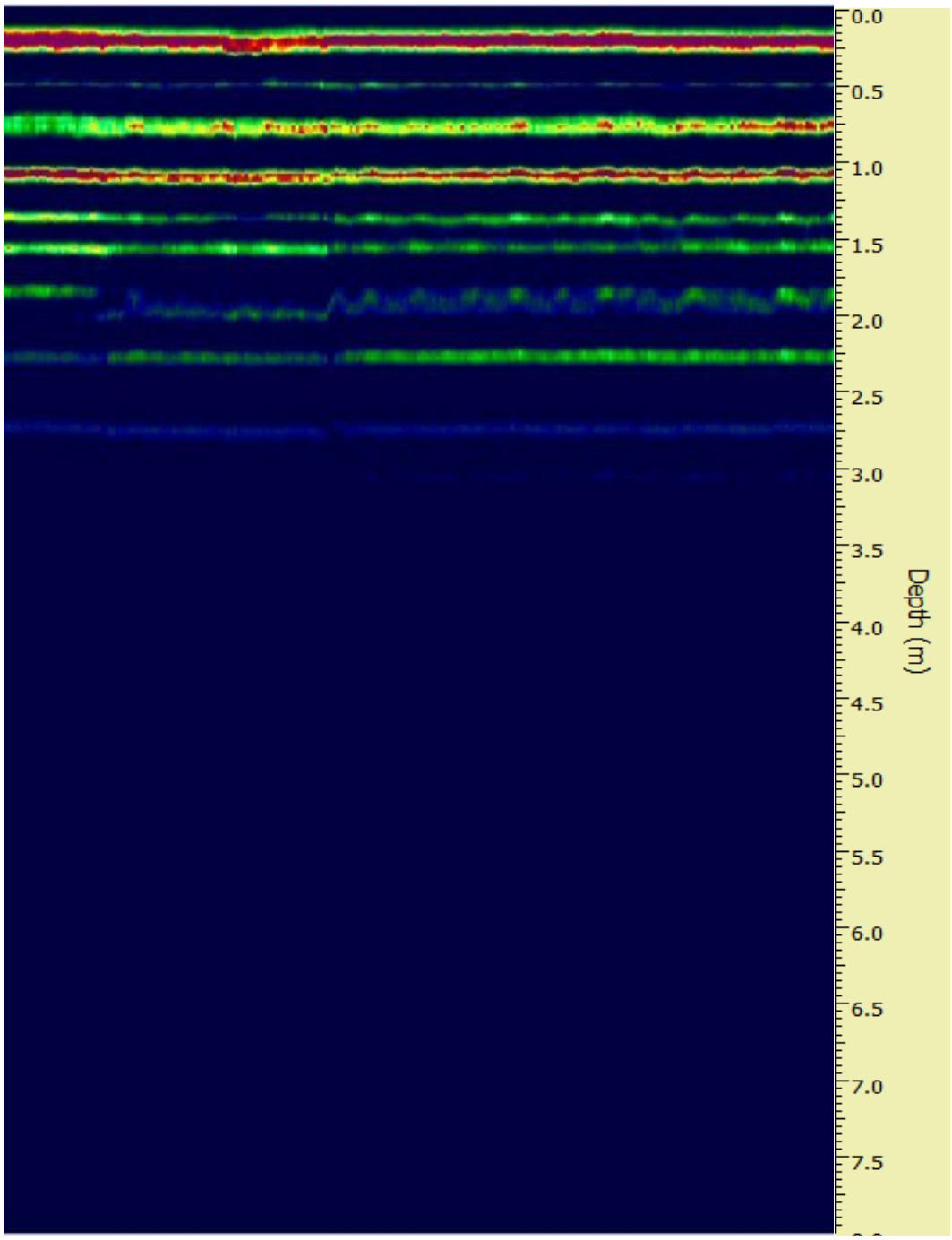

Fig 52: Walking across the road with wall intact at second location

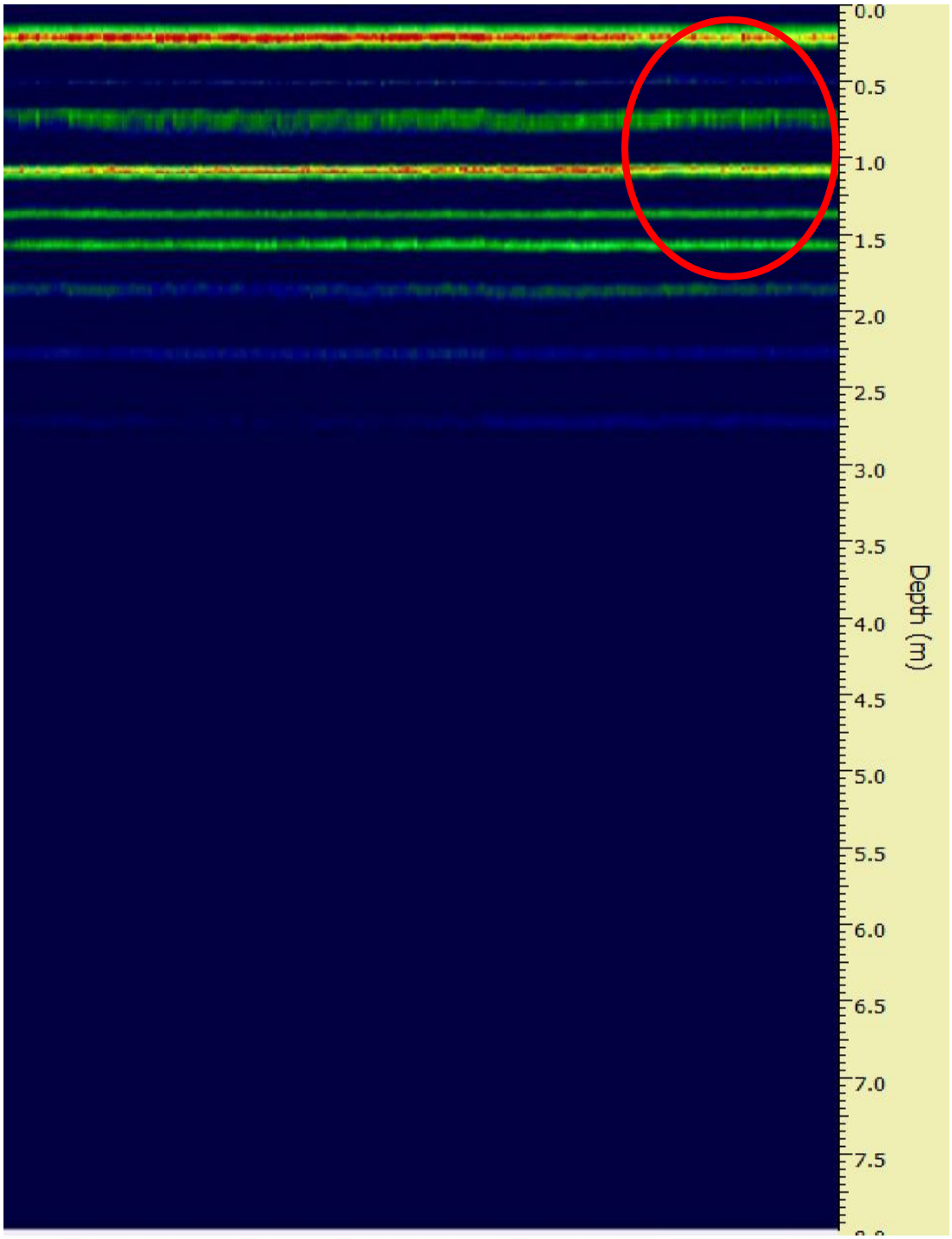

Fig 53: Walking across the road towards the canal where the wall was broken, thicker red line on the left end indicates the water content increases as we move closer to the canal

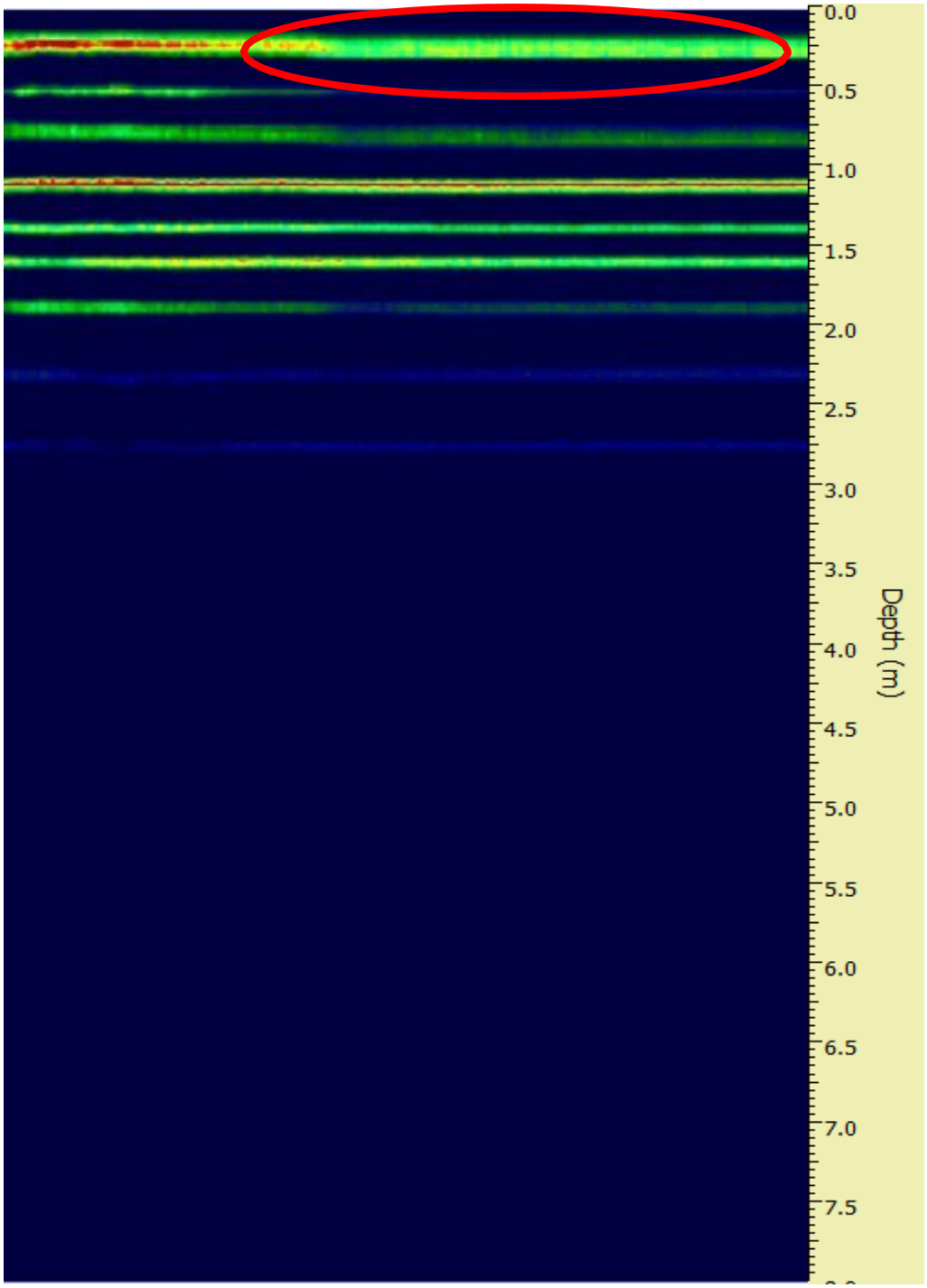

Fig 54: Walking across the road towards the canal where the wall was broken, thicker red line on the left end indicates the water content increases as we move closer to the canal

After this, we also went down to the Navajo Generation Plant in Page Arizona. Fig 54 shows the test paths that we took while we were there. Fig 55 shows a basic layout of what we found there. The electric lines were an estimate as the results were showing sudden peaks around that location. Figure 56 was generated using 3D imaging and just tracking gap as seen in figure 54. This gap can be tracked all along the south end of the pond. While walking on the north end I could see a puddle of water next to the bridge.

Fig 55: GPS tracking of our path taken

Fig 56: Layout of the findings

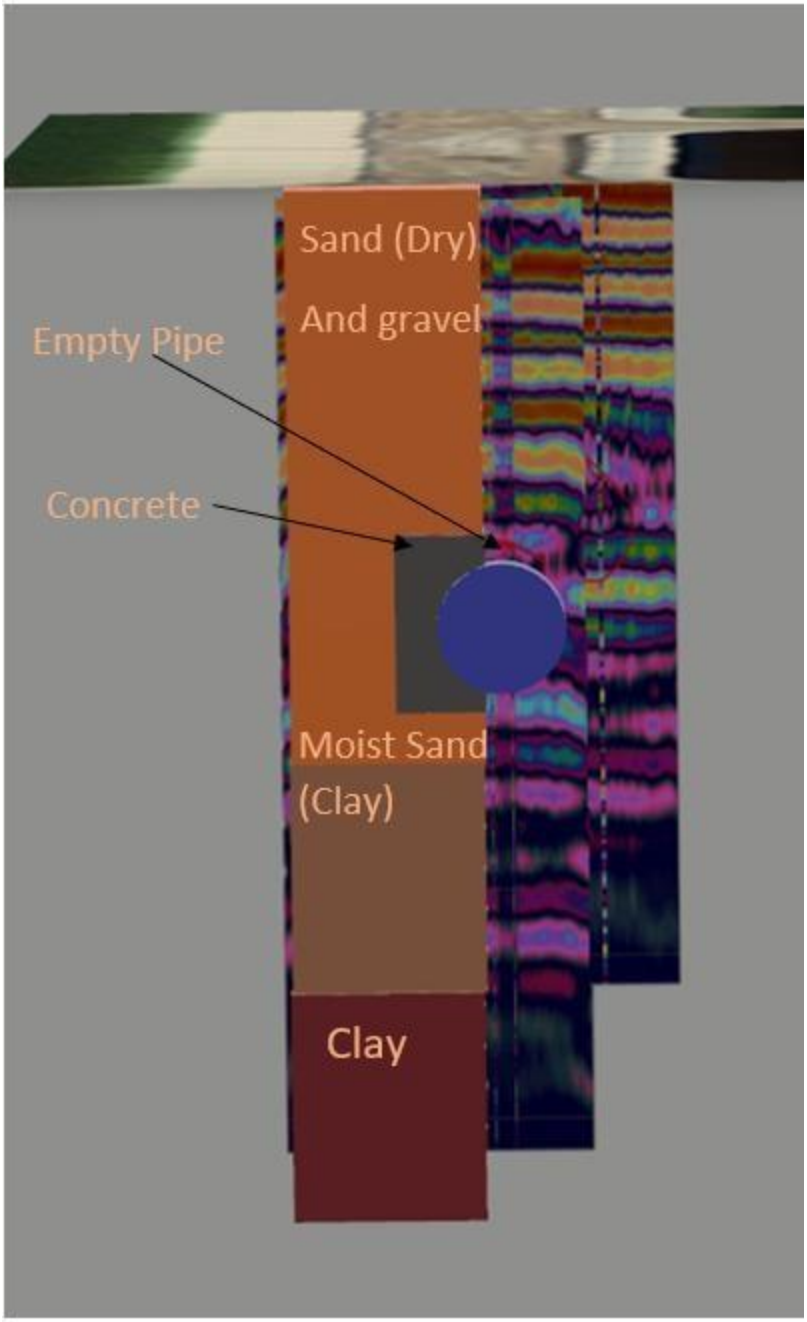

Fig 57: 3D representation of the findings by taking multiple GPR lateral readings across the road between the 2 ponds. Overlaying half of the reading with the solid blocks to indicate what we found.

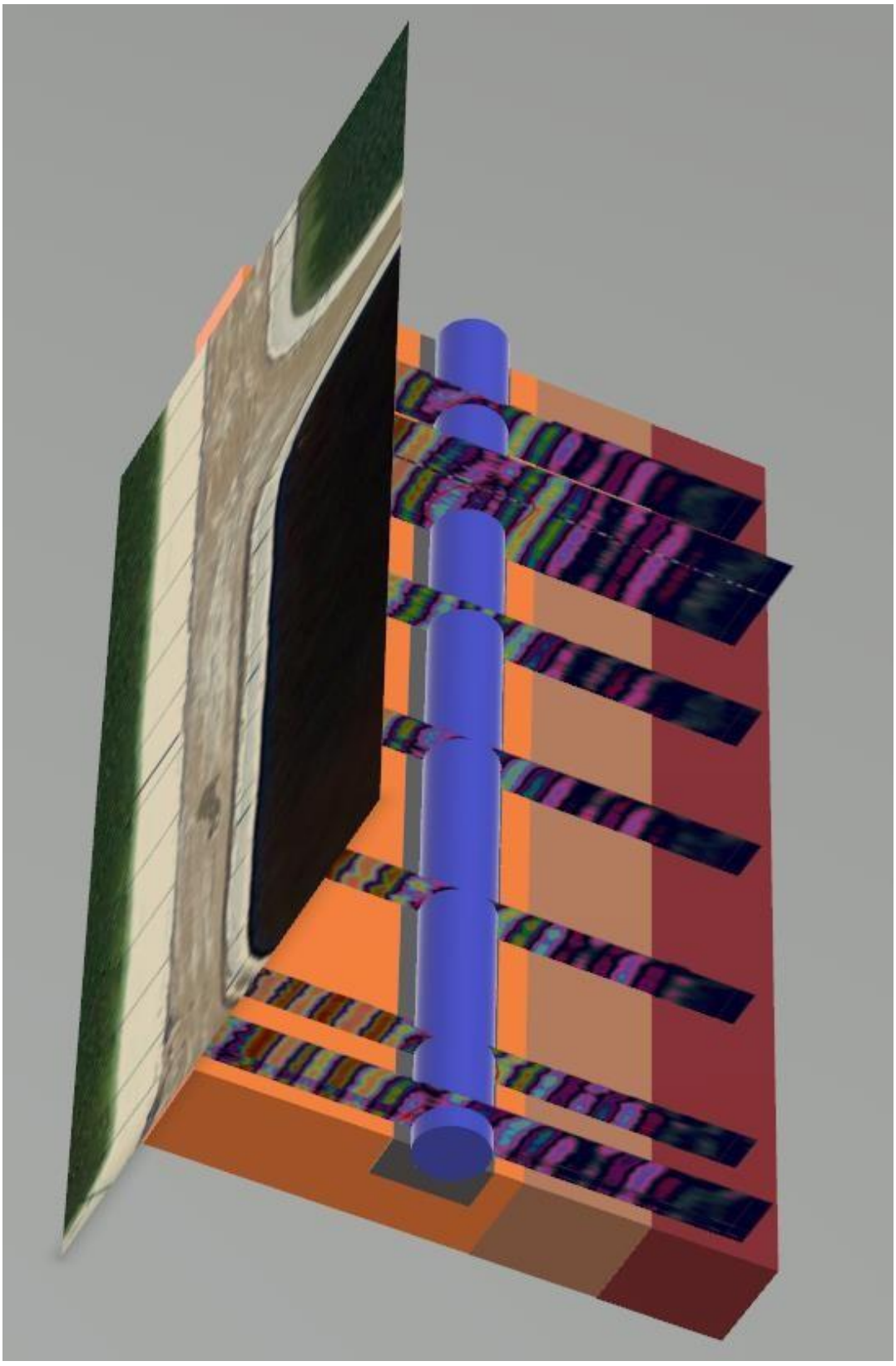

Fig 58: Side view of the 3D view

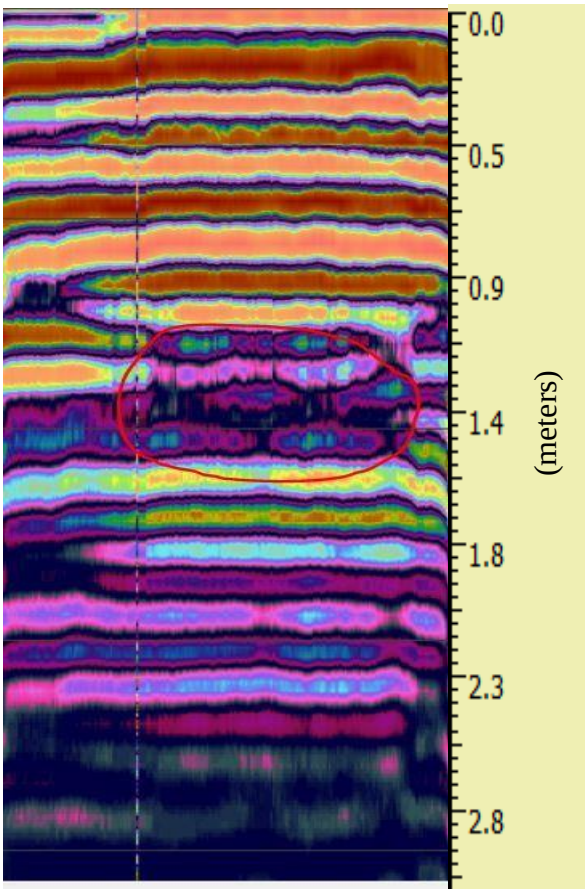

Fig 59: Empty pipe (2ft dia, 3 ft deep)

After all the testing, we can say that GPR can be used as a reliable method to detect leaks. The sensitivity to find small leaks is not there, but by selection of good pathways to do checks to get accurate readings. The technology is not cheap, but it can be used as a preliminary way to find a general location for a leak. The devices can be used through changes or construction. The chances for false alarm, are not very high, and once installed the only maintenance will be needed on the post processing methods.

CHAPTER 4

CONCLUSION

So in conclusion, either method by themselves would not be ideal to be used in complete leak detection. The GPR is ideal for surveying the locations, it is very good at showing any anomalies underground. The acoustic sensor can be very indicative of the type of the leak and the size of the leak, but trying to identify the location of the leak just based on the fourier transforms would not be very accurate. For that purpose, GPR is very indicative of the location where the water would be leaking out of the pipe, either by the irregular thickness of the pipe, or just because of the water surrounding the pipe.

The results from this work if not anything, do indicate a very simple, but effective way of finding leaks. More readings and experiments if done around different flow rate, pressure settings, and material of the pipes, could give us great insight as to how effective it will be around this area.

The frequency of the leaks as can be seen after the transformation shows more response to higher frequencies. This could be attributed to the ratio of the leak size to the diameter of the test section. As seen in the work of (Bull, 1996), the leaks would create a turbulent boundary layer, resulting in high frequency sounds. These results were found by doing spectral analysis and theoretically finding relations between the flow rates, wave numbers and the frequency spectrum. Depending on the part of the boundary layer the frequency spectrum would change(Willmarth, 1975), (Blake, 2017). This would be a result of the huge pressure fluctuations that take place in the boundary layers (Bull, 1996),(Camussi, Guj, & Ragni, 2006).

As of the GPR, the work done by (Eyuboglu, Mahdi, & Al-Shukri, n.d.), GPR

technology can be explored by changing multiple factors. The angle between the radars, the frequency, the sampling rates. Due to our restrictions with our device, we could not dwell into it. A major way to find things through a GPR would be to filter out frequencies, which would be very accurate with a higher frequency, while that would not be able to go deeper. Other ways to do this would be to use a LABview program, but to be accurate in using it we would need to know the commands used to program the device. But for our purpose of surveying, it would still be good to work with lower frequencies which would go deeper, as there will still be some irregularities that could be noticed.

REFERENCES

Brodetsky, I., & Savic, M. (1993). *Leak monitoring system for gas pipelines*. 17–20 vol.3. https://doi.org/10.1109/ICASSP.1993.319424

Butterfield, J. D., Krynkin, A., Collins, R. P., & Beck, S. B. M. (2017). Experimental investigation into vibro-acoustic emission signal processing techniques to quantify leak flow rate in plastic water distribution pipes. *Applied Acoustics*, *119*, 146–155. https://doi.org/10.1016/j.apacoust.2017.01.002

Hunaidi, O, Wang, A., Bracken, M., Gambino, T., & Fricke, C. (n.d.). *Acoustic methods for locating leaks in municipal water pipe networks*. 15.

Hunaidi, Osama, & Chu, W. T. (1999). Acoustical characteristics of leak signals in plastic water distribution pipes. *Applied Acoustics*, *58*(3), 235–254. https://doi.org/10.1016/S0003-682X(99)00013-4

Khulief, Y. A., Khalifa, A., Mansour, R. B., & Habib, M. A. (2012). Acoustic Detection of Leaks in Water Pipelines Using Measurements inside Pipe. *Journal of Pipeline Systems Engineering and Practice*, *3*(2), 47–54. https://doi.org/10.1061/(ASCE)PS.1949-1204.0000089

Lai, W. W. L., Chang, R. K. W., Sham, J. F. C., & Pang, K. (2016). Perturbation mapping of water leak in buried water pipes via laboratory validation experiments with high-frequency ground penetrating radar (GPR). *Tunnelling and Underground Space Technology*, *52*, 157–167. https://doi.org/10.1016/j.tust.2015.10.017

Nakhkash, M., & Mahmood-Zadeh, M. R. (n.d.). *Water Leak Detection Using Ground Penetrating Radar*. 5.

Prego, F. J., Solla, M., Puente, I., & Arias, P. (2017). Efficient GPR data acquisition to detect underground pipes. *NDT & E International*, *91*, 22–31. https://doi.org/10.1016/j.ndteint.2017.06.002

Rocha, H. A. F. (n.d.). *54) ACOUSTIC IMAGING APPARATUS WITH GRAY SCALE DISPLAY*. 9.

Zhang, D. J. (1996). *Designing a Cost Effective and Reliable Pipeline Leak Detection System*. 11.

Blake, W. K. (2017). Essentials of Turbulent Wall Pressure Fluctuations. In *Mechanics of Flow-Induced Sound and Vibration, Volume 2* (pp. 81–177). https://doi.org/10.1016/B978-0-12-809274-3.00002-7

Bull, M. K. (1996). WALL-PRESSURE FLUCTUATIONS BENEATH TURBULENT BOUNDARY LAYERS: SOME REFLECTIONS ON FORTY YEARS OF RESEARCH. *Journal of Sound and Vibration*, *190*(3), 299–315. https://doi.org/10.1006/jsvi.1996.0066

Camussi, R., Guj, G., & Ragni, A. (2006). Wall pressure fluctuations induced by turbulent boundary layers over surface discontinuities. *Journal of Sound and Vibration*, *294*(1–2), 177–204. https://doi.org/10.1016/j.jsv.2005.11.007

Eyuboglu, S., Mahdi, H., & Al-Shukri, H. (n.d.). *DETECTION OF WATER LEAKS USING GROUND PENETRATING RADAR*. 18.

Willmarth, W. W. (1975). Pressure Fluctuations Beneath Turbulent Boundary Layers. *Annual Review of Fluid Mechanics*, *7*(1), 13–36. https://doi.org/10.1146/annurev.fl.07.010175.000305

APPENDIX A

MATLAB CODE FOR ANALYZING THE AUDIO SIGNALS

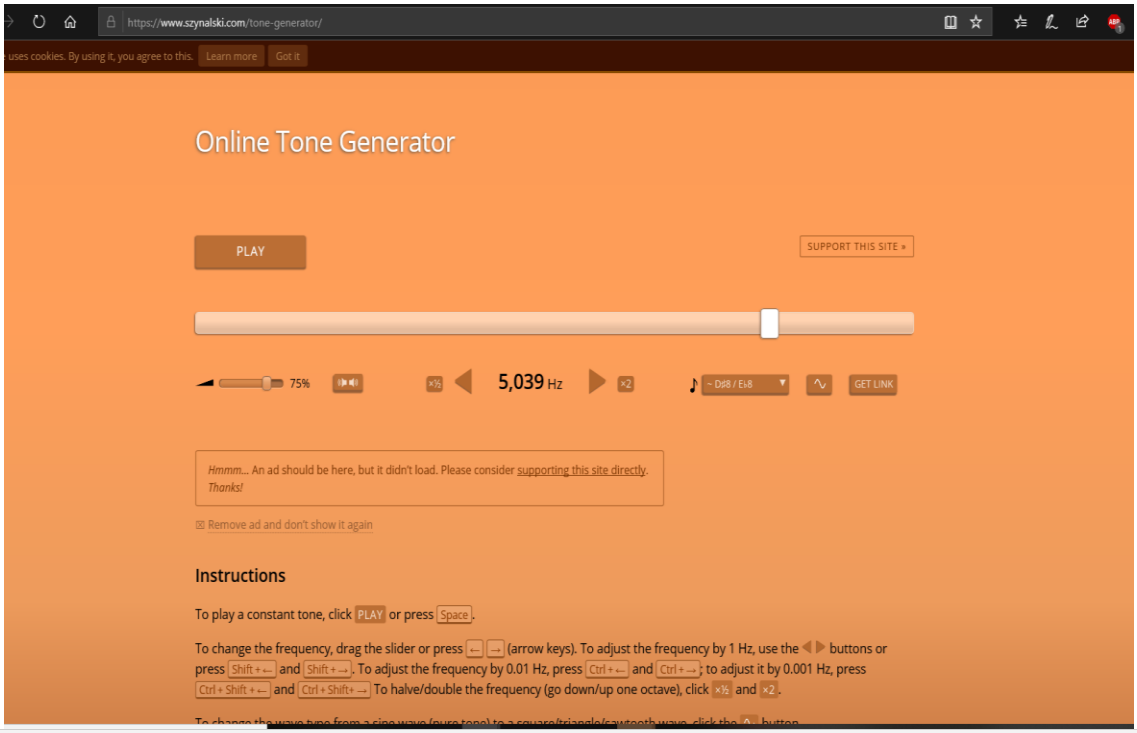


```
clear
clc
close all

addpath('C:\Users\hp\Documents\Sound recordings');

[y,Fs] = audioread('recording (105).m4a');
len=length(y);
T = 1/Fs;             % Sampling period
L = length(y);        % Length of signal
t = (0:L-1)*T;        % Time vector

X=y(:,1);
yrm=mag2db(X);
R=rms(X);

Y = fft(X);

[pxx,fw] = pwelch(X,1000,900,100000,Fs);
px1=10*log10(pxx);
l=length(pxx);
p2 = abs(px1/l);
```

```
figure
plot(fw,px1);
title('Power Spectrum ')
xlabel('Frequency (Hz)')
ylabel('PSD (dB/Hz)')

P2 = abs(Y/L);
P1 = P2(1:L/2+1);
f = (Fs*(0:(L/2))/L);
figure
box on
plot(f,P1) ;
ylim([0 0.001])
title('Frequency Plot ')
xlabel('f (Hz)')
ylabel('|P1(f)|')
```

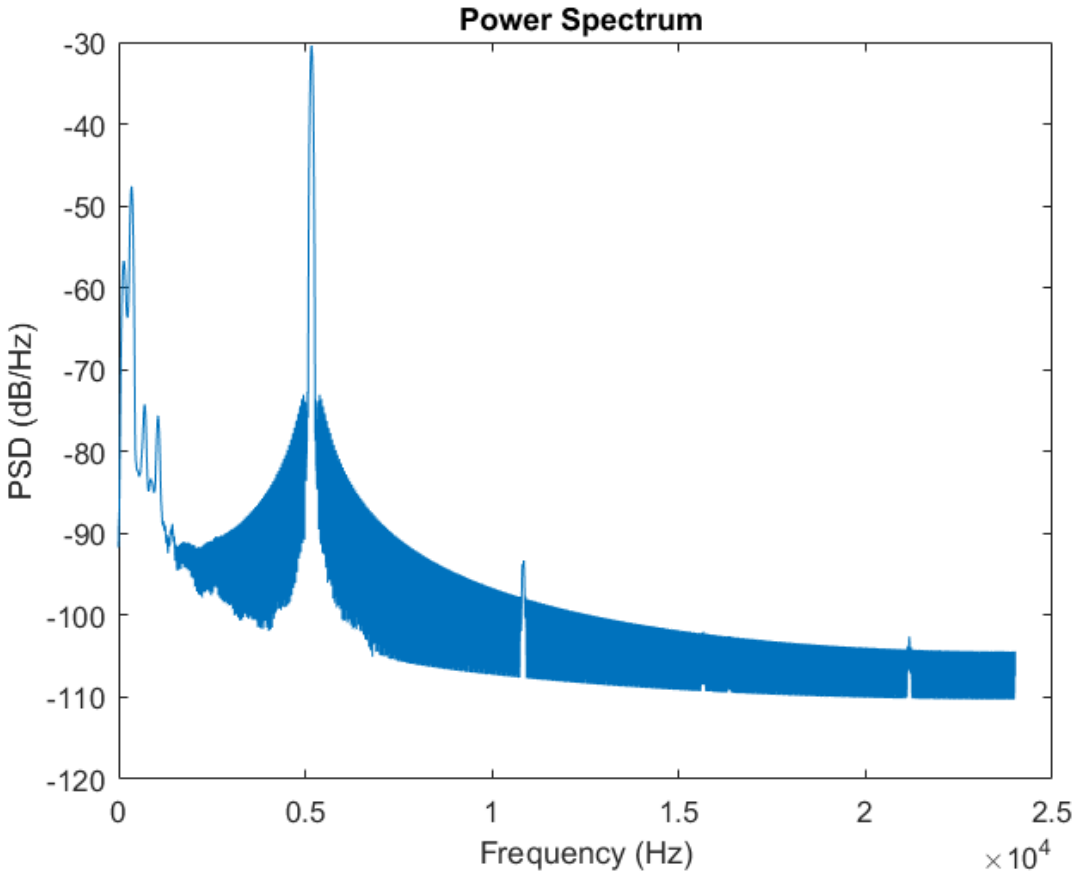

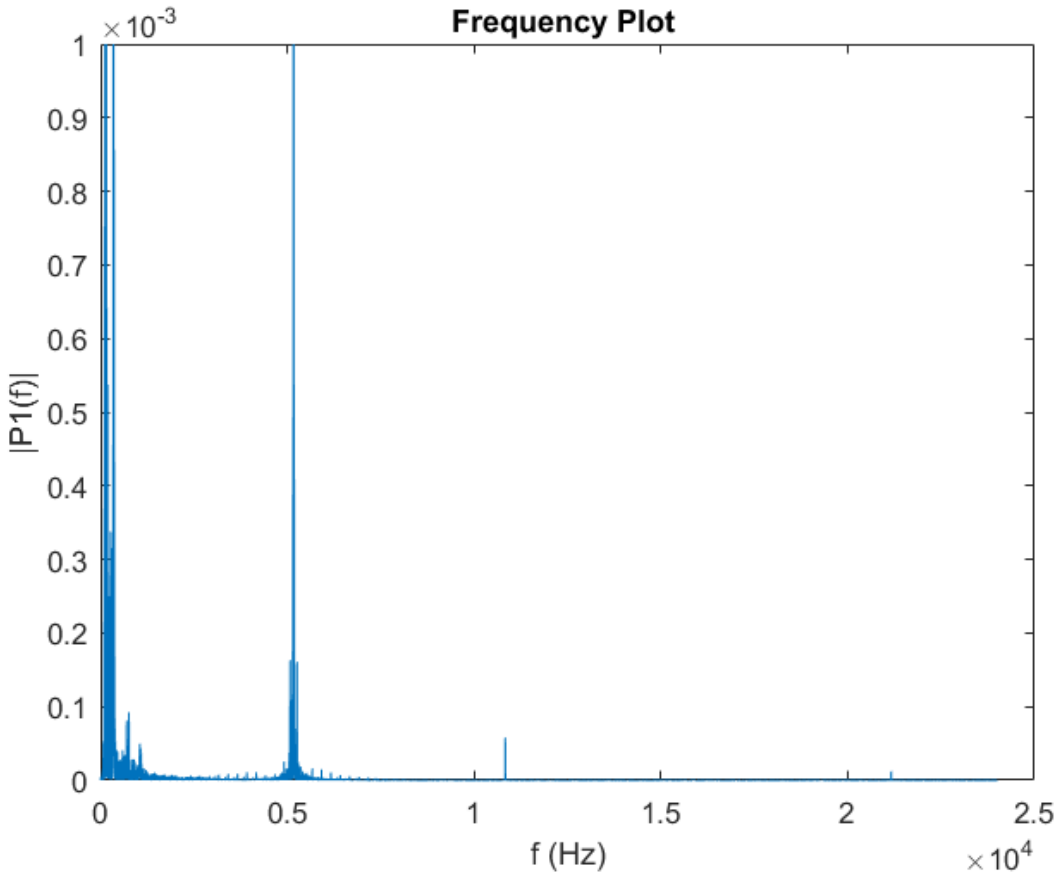

Published with MATLAB® R2017a